Scenarios for the Creation of Hyperchaotic Attractors in 3D Maps

Shykhmamedov A.[1], **Karatetskaia E.**[1],
Kazakov A.[1], **Stankevich N.**[1]

[1] National Research University Higher School of Economics,
25/12 Bolshaya Pecherskaya Ulitsa, 603155 Nizhny Novgorod, Russia

e-mails:
aykhansh@gmail.com;
eyukaratetskaya@gmail.com;
kazakovdz@yandex.ru;
stankevichnv@mail.ru

Abstract

We study bifurcation mechanisms for the appearance of hyperchaotic attractors in three-dimensional diffeomorphisms, i.e., such attractors whose orbits have two positive Lyapunov exponents in numerical experiments. In particular, periodic orbits belonging to the attractor should have two-dimensional unstable invariant manifolds. We discuss several bifurcation scenarios which create such periodic orbits inside the attractor. This includes cascades of supercritical period-doubling bifurcations of saddle periodic orbits and supercritical Neimark-Sacker bifurcations of stable periodic orbits, as well as various combinations of these cascades. These scenarios are illustrated by an example of the three-dimensional Mirá map.

Keywords. Hyperchaotic attractor, homoclinic orbit, three-dimensional map.

1 Introduction

This paper is devoted to the study of bifurcation scenarios leading to the appearance of hyperchaotic attractors in the three-dimensional map

$$\begin{cases} \bar{x} = y, \\ \bar{y} = z, \\ \bar{z} = M_1 + Bx + M_2 z - y^2. \end{cases} \tag{1}$$

Here x, y, and z are phase variables; M_1, M_2, and B are parameters. This map is one of the well-known "homoclinic maps" which were introduced in [34, 35] as normal forms for the first-return maps near homoclinic tangencies of multidimensional systems, see also [32, 37, 38, 44, 86, 87]. The map (1) has the constant Jacobian B. When $B = 0$, the map effectively coincides with the two-dimensional map $\bar{y} = z,\ \bar{z} = M_1 + M_2 z - y^2$. It is the well-known two-dimensional endomorphism introduced and studied by C. Mirá in 60s [65], see also [9]. Therefore, we call map (1) the *three-dimensional Mirá map*. It is worth noting that this map belongs to the class of 3D Hénon maps. In the paper [61] Lomelí and Meiss showed that every quadratic 3D map with a constant Jacobian, whose inverse map is also quadratic, can be reduced to the form $\bar{x} = y,\ \bar{y} = z,\ \bar{z} = Bx + G(y, z)$, where G is a quadratic polynomial in y and z. Therefore, such diffeomorphisms are also called "Lomelí maps", see e.g. [66].

Recall, that the term "hyperchaotic attractor" was introduced by Rössler in [70] for strange attractors with (at least) two directions of exponential instability. Hyperchaoticity of an attractor is quite simple to verify numerically. If numerical experiments show that orbits in the attractor have two or more positive Lyapunov exponents (LE), then the observed attractor is hyperchaotic. It is natural to assume that, in order to be hyperchaotic, an attractor should contain nontrivial hyperbolic subsets whose unstable manifolds have dimension ≥ 2.

Thus, the study of hyperchaotic dynamics in the map (1) looks promising, since in a certain region of the parameter space (region SH$(1, 2)$ in Fig. 8) there is a nontrivial hyperbolic set – a three-dimensional Smale horseshoe – whose unstable manifold is two-dimensional [29]. We ascribe the type (n, m) for hyperbolic periodic orbits with n-dimensional stable and m-dimensional unstable invariant manifolds (where types $(n, 0)$ and $(0, m)$ relate, respectively, to the stable and completely unstable periodic orbits). Then, we can call the above horseshoe as the Smale horseshoe of type (1,2). In the parameter space, along pathways leading from the region where the map has a simple attractor (a stable fixed point) to the region where the horseshoe of type (1,2) exists, one can expect hyperchaotic attractors. Which bifurcations occur along such pathways is the main question of the current paper.

At first, let us recall some facts on strange attractors in the map (1). When $B = 0$, the corresponding two-dimensional Mirá endomorphism has, in certain regions of the (M_1, M_2)-parameter plane, hyperchaotic attractors, the so-called snap-back repellers [63], consisting mainly of completely unstable orbits (with two positive Lyapunov exponents). As was shown in [7], see also [69], for small B these attractors are transformed into hyperchaotic attractors for the three-dimensional diffeomorphism (1), i.e., the tendency for the expansion in two directions persists. When B is not too small (yet $|B| < 1$), the map (1) can demonstrate other types of hyperchaotic attractors, in particular, the so-called *discrete Shilnikov homoclinic attractors* containing a saddle-focus fixed point with

a two-dimensional unstable invariant manifold [26, 27, 31]. These attractors are often observed in multidimensional systems from various applications.[1] In the current paper, we study bifurcation mechanisms for the appearance of hyperchaotic attractors for both cases of small and not very small values of the Jacobian B.

We propose two types of bifurcation scenarios leading to the appearance of hyperchaotic attractors in one-parameter families of three-dimensional maps. First, we outline the main stages of the formation of the so-called discrete *homoclinic attractors* that, according to the definition given in [26, 31], contain only one saddle fixed point along with its unstable invariant manifold (in the case under consideration, the fixed point is either a saddle-focus of type (1,2) or a saddle with two negative unstable multipliers). This part includes only a few local and global (homoclinic or heteroclinic) bifurcations leading from a stable fixed point to a homoclinic attractor containing nontrivial hyperbolic subsets with two-dimensional unstable manifolds.

However, this attractor may not be hyperchaotic, especially at the initial stages of its formation. For the appearance of a strange attractor characterized by two positive Lyapunov exponents, it is necessary that

- the majority of orbits in the attractor should have two-dimensional unstable manifolds.[2]

This problem is in the essence of the second, detailed part of the scenarios. This part is much more complicated and variable, because, unlike the first one, it includes infinite sequences of bifurcations. These bifurcations transform periodic stable and saddle orbits to saddles of type (1,2), paving a way to two positive Lyapunov exponents in numerical experiments.

Hyperchaotic homoclinic attractors.

Suppose that a homoclinic attractor containing a fixed point O of type (1,2) appears. This attractor also contains all homoclinic orbits to the fixed point, i.e., the orbits of the intersection of the stable and unstable manifolds of O. In general case, these intersections are transverse. By the Smale-Shilnikov theorem [73, 78], this implies that the attractor must contain nontrivial hyperbolic subsets whose unstable invariant manifolds are two-dimensional. However, this fact does not automatically lead to hyperchaos, since, as it happens in many cases, the attractor is not hyperbolic and may contain also saddle periodic orbits of type (2,1) (and even periodic sinks which may be invisible in numerical experiments) which together can contribute significantly to the computational value of the averaged Lyapunov exponents.

In particular, this is true for the discrete Shilnikov attractors. Such attractors were introduced and partially studied in the papers [26, 27, 31], where a phenomenological

[1] In particular, such hyperchaotic attractors were found in the models of gas bubbles' dynamics [23], gene represillators [81], in the modified generator of Anischenko-Astakhov [71] and in many other models. In all these models a discrete Shilnikov attractor appears on the corresponding three- or multidimensional Poincaré maps. Moreover, we note that the appearance of such attractors is one of the most typical route to strange attractors in multidimensional systems as a whole.

[2] It is difficult to define the "majority" unambiguously here. However, if we assume a small bounded independent and identically distributed (IID) noise acting on the system, then we can expect a unique stationary measure, and the "majority" will mean a set of full measure. Note that we do have the round-off noise in the numerical experiments, but it is not clear if this kind of noise is well-modeled by IID noise.

scenario for their appearance was also described. The main stages of this scenario are schematically presented in Fig. 6. They are as follows:

(i) a supercritical Neimark-Sacker bifurcation of the stable fixed point O, after which this point becomes a saddle-focus of type (1,2), and a stable invariant curve L appears in a neighborhood of O (Fig. 6b);

(ii) the formation of a Shilnikov whirlpool drawing in almost all orbits from some absorbing domain (Fig. 6c);

(iii) the emergence of a transversal intersection between one-dimensional stable and two-dimensional unstable invariant manifolds of the saddle-focus fixed point O (Fig. 6d).

We consider also another type of discrete homoclinic attractors which contain a saddle fixed point with a pair of negative unstable multipliers. We show how such attractors can appear in one-parameter families of three-dimensional maps. The key steps of the corresponding scenario are as follows:

(i) a supercritical period-doubling bifurcation of a stable fixed point O, after which this point becomes saddle of (2,1)-type (Fig. 2b);

(ii) one more supercritical period-doubling bifurcation of the saddle fixed point O, after which it becomes a saddle of the desired (1,2)-type (Fig. 2c);

(iii) the emergence of a transversal homoclinic intersection between stable and unstable invariant manifolds of O (Fig. 3).

We call the corresponding attractors *hyperchaotic Hénon-like attractors*[3]. Both scenarios are considered in Section 2 where we supplement them by the second, detailed part which is responsible for the appearance of two positive Lyapunov exponents in numerical experiments.

In the papers [48, 84, 85] it was observed in several examples that chaotic attractors can transform to hyperchaotic ones as a result of the absorption of periodic orbits with two-dimensional unstable invariant manifolds into the attractor. We suggest two bifurcation mechanisms leading to such transformations. The first one is associated with infinite cascades of period-doubling bifurcations of saddle periodic orbits of type (2,1) which transform them into orbits of type (1,2). The second mechanism is related to the formation of saddle-focus periodic orbits of type (1,2) via Neimark-Sacker bifurcations of stable periodic orbits. In both cases the absorption of hyperchaotic saddles (of types (1,2)) by the attractor happens via homoclinic or heteroclinic bifurcations.

Hyperchaotic attractors in the map (1)**.**

In the second part of the paper (Sections 4–5), we apply the proposed scenarios to study mechanisms for the appearance of hyperchaotic attractors in the three-dimensional Mirá map (1). We consider cases of small and not very small values of the Jacobian B. In both cases we start from a stable fixed point O_+ which appears via a saddle-node bifurcation together with a saddle fixed point O_- of type (2,1) and change parameters

[3]In three-dimensional maps another type of "Hénon-type" attractors is also possible. They appear as a result of a sequence of period-doubling bifurcations of a stable invariant curve, and were called *quasiperiodic Hénon-like attractors* in [13–15] by analogy with Hénon-like attractors.

towards the region SH(1,2), see Fig. 8, where the Smale horseshoe of type (1,2) exists [29].

The first bifurcation along this pathway is always the supercritical Neimark-Sacker bifurcation after which the point O_+ becomes saddle-focus of type (1,2) and a stable invariant curve L is born in its neighborhood. Further, this curve breaks down, giving rise to a certain chaotic attractor (with only one positive Lyapunov exponent), but later this attractor becomes hyperchaotic. The study of accompanying bifurcations is the main focus of this part of the paper.

We note that usually, before the destruction, the curve L becomes resonant: a pair of period-q stable and saddle-(2,1) orbits appears on it (inside the corresponding Arnold tongue); in this case the resonant curve is the closure of the unstable manifold of the period-q saddle orbit.

In the paper we pay special attention to the cases of the so-called *strong resonances 1:3 and 1:4* which are the most difficult and interesting. Besides, their influence on the organization of the corresponding bifurcation diagrams is the most visible (see e.g. Lyapunov diagrams for the map under consideration in Fig. 10, where codimension-two points giving rise to the Arnold tongues with the strong resonances 1:3 and 1:4 are denoted by R_3 and R_4, respectively). In the case of two-dimensional diffeomorphisms, the nondegenerate 1:3 resonance usually leads to the global instability [76], the corresponding invariant curve breaks down without the appearance of stable elements of dynamics. However, this is no longer true for the three-dimensional maps with not small values of the Jacobian. In particular, as is shown in [26, 31], regular and chaotic attractors can appear in the map (1) after the destruction of the curve L near the 1:3 resonance. We show that these attractors can be even hyperchaotic. However, they occupy very thin regions in the parameter space, and can appear only for specific values of the Jacobian B, see the red-colored regions below the point R_3 in Fig. 10d.

As for the 1:4 resonance, we show that, unlike the 1:3 resonance, it is responsible for the emergence of the most visible Arnold tongue with stable dynamics. Inside this tongue, the resonant period-4 stable and saddle-(2,1) orbits undergo numerous bifurcations. Moreover, a type of these bifurcations strongly depends on the value of the Jacobian B.

For small values of B, these bifurcations include a cascade of period-doubling bifurcations resulting in a four-component Hénon-like attractor containing infinitely many saddle orbits of type (2,1), see Fig. 14b. These orbits, as well as the resonant period-4 saddle orbit, also undergo cascades of period-doubling bifurcations leading to the formation of a hyperchaotic attractor containing infinitely many periodic saddle orbits of type (1,2), see Section 4 for more detail.

The stable period-4 orbit can also undergo the supercritical Neimark-Sacker bifurcation followed by the creation of a four-component discrete Shilnikov attractor. This scenario of the transition to hyperchaos is more typical for the cases of not small values of the parameter B ($B \in [0.3, 0.6]$ in Fig. 17b). Independently of this, the resonant period-4 saddle orbit (of type (2,1)), as in the case of small B, undergoes an infinite cascade of period-doubling bifurcations leading to the creation of a nontrivial hyperbolic subset of type (1,2). Then, a new type of hyperchaotic attractor can appear when this subset or its parts are absorbed by the above mentioned four-component Shilnikov attractor. After this absorption event, the four-component attractor transforms into a one-component attractor containing both the saddle-focus and saddle period-4 orbits of type (1,2), see Section 5 for more detail.

In the last part of the paper (Section 6), we demonstrate another scenario of the destruction of the curve L. We show that for not small values of the Jacobian (e.g. for $B = 0.7$) this curve can undergo a quite long sequence of period-doubling bifurcations resulting in the formation of a chaotic attractor with one positive, one near-zero (indistinguishable from zero in the numerics) and one negative Lyapunov exponent. We discuss and explain this phenomenon.

2 Scenarios for the appearance of hyperchaotic attractors

In this section, we describe scenarios leading to the appearance of hyperchaotic attractors in three-dimensional maps. Let us consider a one-parameter family of the three-dimensional maps

$$\bar{x} = F(x, \varepsilon)$$

depending on a parameter ε. In the presented below scenarios, we start with a fixed point O which is asymptotically stable and belongs to some absorbing domain $D_a(O)$, see Fig. 2a. Finally, as a result of a series of codimension-one bifurcations, we obtain a homoclinic attractor containing the point O which becomes a saddle or a saddle-focus with a two-dimensional unstable invariant manifold. We also pay special attention to the cascades of bifurcations due to which the majority of orbits inside the attractor get two-dimensional unstable invariant manifolds.

2.1 Hyperchaotic Hénon-like attractor

The *hyperchaotic Hénon-like attractor* is a homoclinic attractor containing a saddle fixed point with a pair of negative unstable multipliers. It can appear as a result of the scenario the beginning part of which coincides with the well-known scenario of the birth of the Hénon attractor. Therefore, let us first recall some details on the Hénon and Hénon-like attractors and scenarios for their appearance.

2.1.1 Some details about Hénon-like attractors

The Hénon attractor is a homoclinic attractor of the two-dimensional Hénon map $H : \bar{x} = y,\ \bar{y} = M - bx - y^2$ [45]. It contains the saddle fixed point O with a negative unstable multiplier and is formed after the Feigenbaum cascade of period-doubling bifurcations [18, 22, 62] followed by a cascade of heteroclinic "band-merging" bifurcations [77]. Let us denote the stable and unstable multipliers of the point O by λ and γ. Then, for the Hénon attractor, the following conditions always hold: $\gamma < -1$ (the unstable multiplier is negative) and $\sigma = |\gamma\lambda| < 1$ (area-contracting condition). Depending on the sign of the stable multiplier λ, the Hénon attractor can be of two types: if $-1 < \lambda < 0$ the attractor is orientable, see the example of its phase portrait in Figure 1a; and if $0 < \lambda < 1$ the attractor is nonorientable, see the phase portrait in Figure 1c (exactly this attractor was discovered and studied by M. Hénon in [45]).

When dynamics in the map are associated with the existence of the Hénon attractor[4], this attractor, together with the saddle point O, also contains the unstable manifold

[4]The question of the existence of the Hénon attractor is very delicate. For sufficiently small positive

$W^u(O)$ and homoclinic points h_i to O, i.e, such points where $W^u(O)$ intersects with the stable manifold $W^s(O)$. Figures 1b and 1d show schematic representations of the homoclinic structure for the orientable and nonorientable Hénon attractors, respectively. Let us briefly describe them.

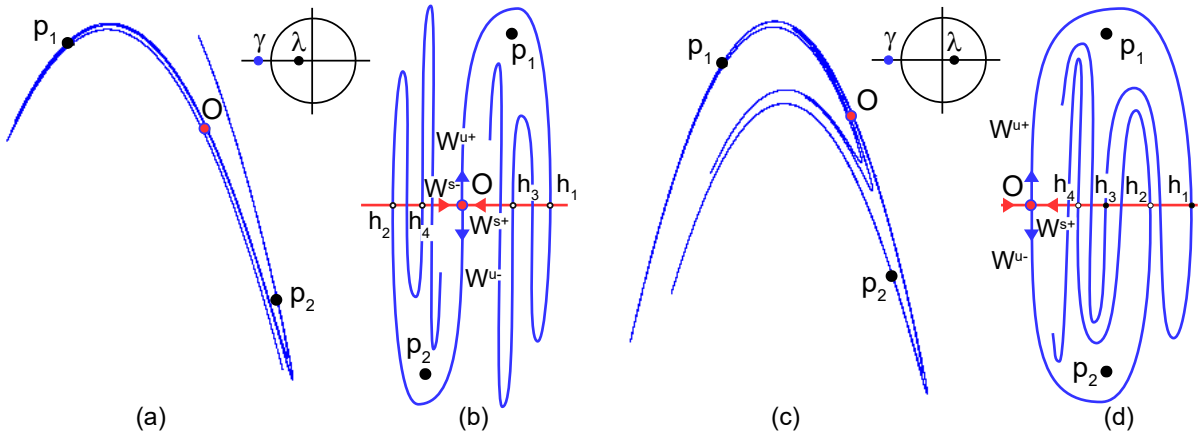

Figure 1: (a) Orientable Hénon attractor in the map H for $b = 0.3, M = 2.1$ and (c) its homoclinic structure; (b) nonorientable Hénon attractor in the map H for $b = -0.3, M = 1.4$ and (d) its homoclinic structure. O is a saddle fixed point belonging to the attractor; W^{s+} and W^{s-}, W^{u+} and W^{u-} are the pairs of stable and unstable separatrices of O, p_1 and p_2 are the components of a period-2 orbit which appears after the period-doubling bifurcation of the point O, and $h_1, h_2, h_3, \ldots$ are the points of homoclinic intersections $W^u(O) \cap W^s(O)$.

The unstable invariant manifold $W^u(O)$ is divided by the point O into two connected components – separatrices W^{u+} and W^{u-}. Since the unstable multiplier γ of O is negative ($\gamma < -1$), the separatrices W^{u+} and W^{u-} are invariant under H^2 and such that $H(W^{u+}) = W^{u-}$ and $H(W^{u-}) = W^{u+}$. This implies that points of W^u jump under iterations of H alternately from one separatrix to another.

The stable manifold $W^s(O)$ is also one-dimensional and it is divided by the point O into two separatrices W^{s+} and W^{s-}. For the orientable Hénon attractor, the stable multiplier λ is negative and thus, as for the unstable manifold, $H(W^{s+}) = W^{s-}$ and $H(W^{s-}) = W^{s+}$.

Let h_1 be an intersection point of W^{u+} with W^{s+}. Then, h_2 is an intersection point of W^{u-} with W^{s-}, since $H(W^{u+}) = W^{u-}$ and $H(W^{s+}) = W^{s-}$; h_3 is again an intersection point of W^{u+} with W^{s+}, etc. Correspondingly, the points $h_1, h_2, ...$ are homoclinic points of some homoclinic to O orbit. Here, the points with odd indices $h_1, h_3, ...$ belong to the separatrix W^{s+}, while the points with even indices $h_2, h_4, ...$ belong to W^{s-}, see Fig. 1b. For the nonorientable Hénon attractor, multiplier λ is positive and, thus, all homoclinic points $h_1, h_2, ...$ belong to one stable separatrix (e.g. W^{s+}) jumping from one unstable separatrix to another, see Fig. 1d.

values of the Jacobian of the Hénon map, Benedicks and Carleson proved in [10] that the set of parameter values corresponding to the chaotic attractor is a Cantor set with the positive Lebesgue measure. Moreover, the set of parameter values corresponding to stable periodic orbits is dense in any neighborhood of parameters with the chaotic attractor. For sufficiently large values of the Jacobian (very close to the classical Hénon's parameters) an analogous result was obtained in [21] by means of computer-assisted proof methods. Thus, for specific parameter values, one can never be sure whether the chaotic attractor is observed or it is just a transient chaos, after which orbits will run to some stable periodic orbit with an extremely narrow absorbing domain.

Similar homoclinic attractors are observed in many two-dimensional and multidimensional maps, as well as in Poincaré maps for various multidimensional systems of differential equations. Further, we will call them *Hénon-like attractors*. More precisely the Hénon-like attractor can be defined as a homoclinic attractor containing the saddle fixed point (periodic orbit in the case of systems of differential equations) with a negative unstable multiplier and $\sigma < 1$.

2.1.2 General outline of the scenario for hyperchaotic Hénon-like attractor appearance

We start with the general outline of the scenario leading to the appearance of hyperchaotic Hénon-like attractor purposely skipping some details (accompanying bifurcations) which will be given in the framework of the second part of the scenario in Sec. 2.1.3.

As for the Hénon attractor, the first step in the framework of the scenario is the supercritical period-doubling bifurcation occurring with the stable fixed point O. Suppose that it happens at $\varepsilon = \varepsilon_{PD}$. After this bifurcation, the point O becomes saddle of (2,1)-type and a stable period-2 orbit (p_1, p_2) appears in its neighborhood, see Figure 2b. The saddle point O has the following set of multipliers: $\gamma < -1, -1 < \lambda_1 < 0$ and $|\lambda_2| < 1$. The unstable invariant manifold $W^u(O)$, separated by the point O into two separatrices W^{u+} and W^{u-}, is a segment with endpoints p_1 and p_2. Since this manifold corresponds to the negative multiplier $\gamma < -1$, we have a semi-local symmetry between the pair of separatrices W^{u+} and W^{u-} ($F(W^{u+}) = W^{u-}$ and $F(W^{u-}) = W^{u+}$). The stable invariant manifold W^s corresponds to a pair of real multipliers λ_1 and λ_2. Suppose that $|\lambda_1| > |\lambda_2|$, i.e., λ_1 corresponds to the leading direction W^{ls}, and λ_2 – to the strong stable manifold W^{ss} tangent to the eigenvector corresponding to λ_2. Then, $\lambda_2 > 0$ if the map F is orientable and $\lambda_2 < 0$, otherwise. Here, we consider only the case of orientation-preserving maps.

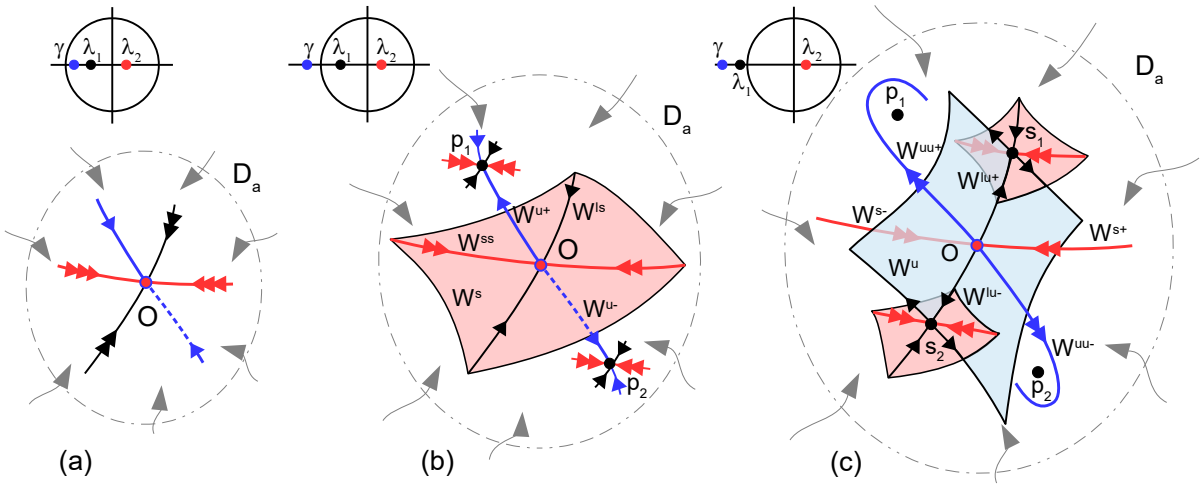

Figure 2: Main bifurcations toward the hyperchaotic Hénon-like attractor appearance. (a) O is a stable fixed point, it resides in some absorbing domain D_a; (b) period-doubling bifurcation of the point O occurs: a stable period-2 orbit (p_1, p_2) is born, while the point O becomes saddle with a negative unstable multiplier; (c) period-doubling bifurcation of the saddle point O occurs: a saddle period-2 orbit (s_1, s_2) is born, while the point O becomes saddle with a pair of negative unstable multipliers. In the upper insets the schematic location of the multipliers γ, λ_1, and λ_2 of O is presented.

Remark 1 *The first step in the framework of this scenario is the same as for the creation of the so-called discrete Lorenz and figure-eight homoclinic attractors [26, 27, 36]. Both these attractors are remarkable since they can be pseudohyperbolic [82, 83]. Pseudohyperbolicity is a generalized version of hyperbolicity. Chaotic dynamics of pseudohyperbolic attractors persist under small perturbations (as for hyperbolic attractors), despite the possible occurrence of homoclinic tangencies inside them. Note that the saddle fixed point belonging to both discrete Lorenz and figure-eight attractors should be area-expanding, which means that* $\sigma = \gamma\lambda_1 > 1$.

The next principal bifurcation in the framework of the scenario is a second supercritical period-doubling bifurcation of the saddle fixed point O. Suppose that it occurs at $\varepsilon = \varepsilon^{PD}$. After this bifurcation, the point O becomes saddle of (1,2)-type a period-2 saddle orbit (s_1, s_2) of (2,1)-type appears in its neighborhood, see Figure 2c. For $\varepsilon > \varepsilon^{PD}$, both unstable multipliers γ and λ_1 of the point O are negative, while the stable multiplier λ_2 is positive since we consider the orientable case. The following conditions on the multipliers are met here

$$\gamma < \lambda_1 < -1,\ 0 < \lambda_2 < 1.$$

A restriction F_u of the initial map F into the local unstable manifold $W^u_{loc}(O)$ has a fixed point $\tilde{O} = O \cap W^u_{loc}$ which is the unstable node with a pair of multipliers $\gamma < \lambda_1 < -1$. Thus, in W^u_{loc}, there are a strong unstable invariant manifold W^{uu}, which is tangent to the eigenvector corresponding to the unstable multiplier γ, and a leading unstable direction W^{lu} corresponding to the multiplier λ_1. Also note that the curves W^{uu} and W^{lu} divide W^u_{loc} into four parts Π_1, Π_2, Π_3, and Π_4 and, since both multipliers of $\tilde{O}$ are negative, $F_u(\Pi_1) = \Pi_3$, $F_u(\Pi_3) = \Pi_1$, $F_u(\Pi_2) = \Pi_4$, and $F_u(\Pi_4) = \Pi_2$. All orbits in W^u_{loc}, except those that belong to W^{uu}, tend to the node $\tilde{O}$ (in backward time) along the smooth cubic parabola-like curves. These curves are tangent to the leading direction W^{lu} of $\tilde{O}$, see Fig. 3a. If $h_1 \in \Pi_1$ is one of such points, then each its odd (even) iteration under F_u^{-1} tends to $\tilde{O}$ along right (left) branch of this parabola-like curve staying in Π_3 (Π_1). It is important to note that since, by the moment, only orbits belonging to $W^s(O)$ tend to the saddle fixed point O, for other orbits there is no mechanism to return into a neighborhood of this point.

We suppose that such mechanism appears at $\varepsilon = \varepsilon^H$ due the emergence of a homoclinic orbit to O, see Fig. 3b, when the stable manifold $W^s(O)$, separated by the point O into two separatrices W^{s+} and W^{s-}, starts to intersect with the unstable manifold $W^u(O)$. Suppose that h_1 is the first intersection point of W^{s+} with W^u at Π_1, see Figure 3a. Then (since $F^{-1}(W^{s+}) = W^{s+}$ and $F_u(\Pi_1) = \Pi_3$), $h_2 = F^{-1}(h_1)$ is the intersection point of the same stable separatrix W^{s+} with W^u in Π_3; $h_3 = F^{-1}(h_2)$ is again an intersection point of W^{s+} with W^u in Π_1, etc. Correspondingly, the points $h_1, h_2, ...$ are homoclinic points of some homoclinic to O orbit, see Figure 3b.

At $\varepsilon > \varepsilon^H$, this homoclinic orbit gives a nontrivial hyperbolic subset of (1,2)-type which, we suppose, becomes attractive, i.e., we get the hyperchaotic Hénon-like attractor inside the absorbing domain $D_a(O)$. If numerically obtained orbits in the attractor spend a sufficiently long time near the hyperbolic subset of (1,2)-type, then a pair of Lyapunov exponents becomes positive, i.e., we observe hyperchaos in numerical experiments[5].

[5]The described hyperchaotic attractor typically is not hyperbolic. Together with periodic saddle orbits of (1,2)-type it also contains periodic saddle orbits of (2,1)-type and homoclinic (heteroclinic) tangencies

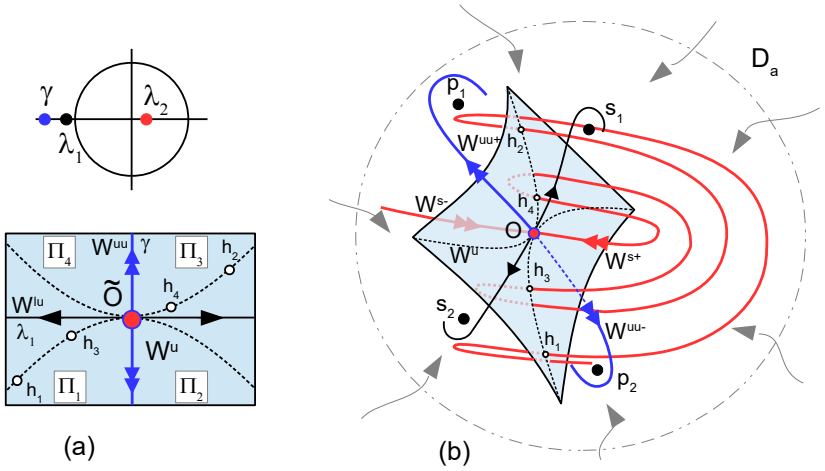

Figure 3: Continuation of Fig. 2: (a) schematic representation of the local unstable manifold $W^u_{loc}(O)$ on which the point $\tilde{O}$ is an unstable node; (b) schematic representation of the homoclinic structure for the hyperchaotic Hénon-like attractor.

In the following section, we show how hyperchaotic Hénon-like attractors can naturally appear in multidimensional systems demonstrating cascades of supercritical period-doubling bifurcations. In Sec. 2.2.2, we generalize this scenario to the case of attractors developing from stable periodic orbits which occur inside Arnold tongues. In Section 4, we demonstrate its implementation inside the Arnold tongues in the three-dimensional Mirá map (1).

2.1.3 Detailed scenario for hyperchaotic Hénon-like attractor appearance

Here we show how the attractor described above can appear in multidimensional systems demonstrating transition to chaos via cascades of period-doubling bifurcations. Suppose that, at $\varepsilon = \varepsilon_H$, a Hénon-like attractor appears after a cascade of period-doubling bifurcations followed by a cascade of heteroclinic band-merging bifurcations, see Figure 4. For one-dimensional maps the exponential convergence of these bifurcations is well-known fact [16, 19, 56]. For two-dimensional maps such universality is proved in Refs. [18, 62]. As we know, for three-dimensional maps there are no rigorous results on this topic. However it is believed that the exponential convergence with the same universal property is also observed in this case [17].

A homoclinic structure for the Hénon-like attractor is shown schematically in Figure 5a (left panel). Here, as in the two-dimensional case, the unstable multiplier γ of the fixed point O is negative ($\gamma < -1$) and the stable ones λ_1 and λ_2 are real. Depending on the signs of stable multipliers, homoclinic structures for the Hénon-like attractor can be of four possible types (two in orientable and two in nonorientable cases). Here we consider only one orientable case characterizing by the following values of multipliers $\gamma < -1 < \lambda_1 < 0 < \lambda_2 < 1, |\lambda_2| < |\lambda_1|$ (see the schematic location of the multipliers at the top-right insert of Fig. 5a). This attractor is a three-dimensional generalization of the

between invariant manifolds of various saddles. Moreover, it is possible to show that such attractors also contain heterodimensional cycles connecting these saddles [57–59]. Such cycles robustly persist under small perturbation of the system guaranteeing the presence of a nontrivial hyperbolic subset of (1,2)-type.

classical orientable Hénon attractor.

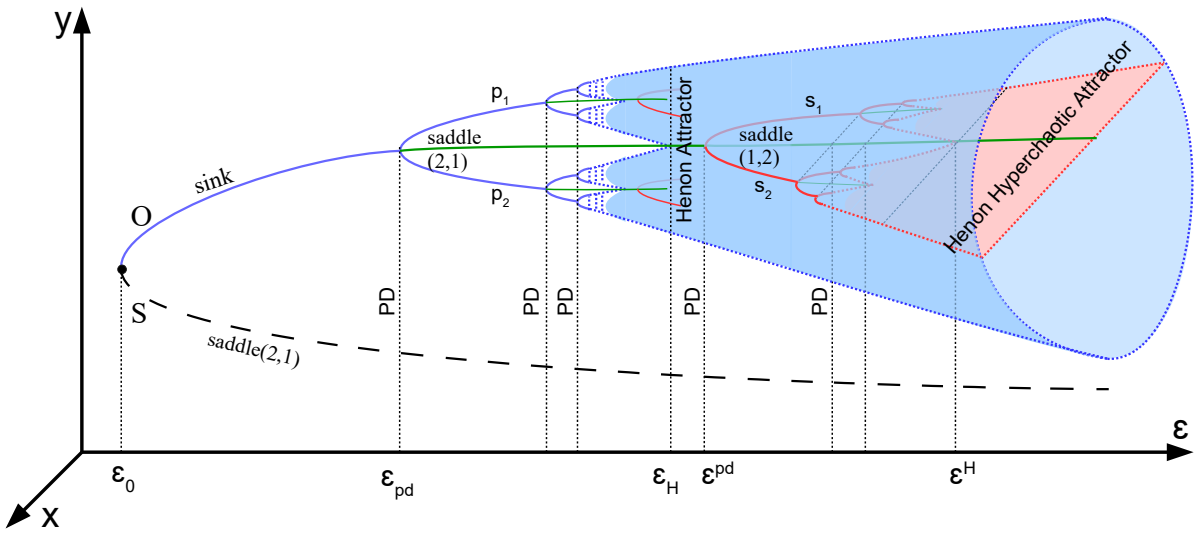

Figure 4: Detailed scenario for the hyperchaotic Hénon-like attractor appearance as a result of a cascade of period-doubling bifurcations of the stable fixed point O followed by cascades of period-doubling bifurcations of periodic saddle orbits of (2,1)-type.

Here the stable invariant manifold $W^s(O)$ is two-dimensional. The restriction F_s of the initial map F into $W^s_{loc}(O)$ has a fixed point $\tilde{O} = O \cap W^s_{loc}$ which is a stable node with a pair of multipliers λ_1 and λ_2. According to the condition $|\lambda_1| > |\lambda_2|$, in W^s_{loc} there are the strong stable invariant manifold W^{ss}, which is tangent to the eigenvector corresponding to $\lambda_2 > 0$, and the leading direction W^{ls} corresponding to $\lambda_1 < 0$. The curve W^{ss} divides W^s_{loc} into two parts Π_1 and Π_2, and, since the leading multiplier is negative ($\lambda_1 < 0$), $F_s(\Pi_1) = \Pi_2$ and $F_s(\Pi_2) = \Pi_1$. All orbits in W^s_{loc}, except those that belong to W^{ss} tend to the node $\tilde{O}$ along the parabola-like curves which are tangent to the leading direction W^{ls}, see the right panel in Fig. 5a. If we take some point h_1 belonging to one such curves p_c and consider its images under F_s, we obtain an orbit $h_1, h_2, ...$ tending to $\tilde{O}$ on one (e.g. right) side of W^{ls} and jumping from one branch of p_c to another after each iteration. Suppose, h_1 is the intersection point of W^{u+} with W^s at its upper part Π_1. Then, (since $F(W^{u+}) = W^{u-}$ and $F_s(\Pi_1) = \Pi_2$) $h_2 = F(h_1)$ is the intersection point of W^{u-} with W^s in its bottom part Π_2; $h_3 = F(h_2)$ is again an intersection point of W^{u+} with W^{s+} in Π_1, etc.

Then, we suppose that the saddle point O of (2,1)-type undergoes a cascade of period-doubling bifurcations, see the schematic phase portrait after the first period-doubling bifurcation in Figure 5b. After each such bifurcation, the periodic orbit gets the two-dimensional unstable manifold and a double-period orbit of (2,1)-type appears in its neighborhood. Then, we suppose that the period-2^n saddle orbits of (2,1)-type emerging after the corresponding period-doubling bifurcations, as well as other saddles of (2,1)-type inside the attractor, also undergo full cascades of period-doubling bifurcation after which all these orbits become of (1,2)-type. It is natural to assume that these cascades have the same universal properties of the exponential convergence as the cascades for stable periodic orbits [17]. We assume that after it, we obtain a hyperchaotic attractor which consists of (infinitely) many components separated by isolated periodic saddles of (1,2)-type (similar to chaotic attractor in the Hénon map before the cascade of heteroclinic

band-merging bifurcations).

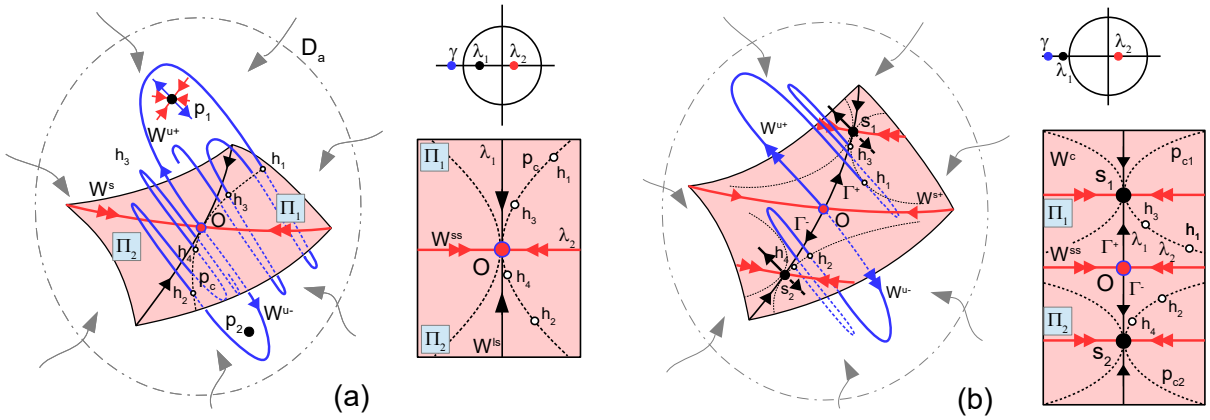

Figure 5: (a) Schematic representation of the homoclinic structure for the Hénon-like attractor of a three-dimensional map; (b) invariant manifolds after the period-doubling bifurcation of the saddle fixed point O.

Further, we suppose that this multi-component attractor goes through a cascade of heteroclinic band-merging bifurcations. These bifurcations are similar, in a sense, to those ones which lead to the pairwise merger of components of a chaotic attractor arising after the successive cascade of period-doubling bifurcations within the second part of the scenario resulting in the birth of the Hénon-like attractor. After each such bifurcation, the number of components decreases by a factor of two.

The final bifurcation here, resulting in the merger of last two components, leads to the emergence of the homoclinic intersections between $W^s(O)$ and $W^u(O)$. As a result, the hyperchaotic Hénon-like attractor appears at $\varepsilon = \varepsilon^H$. Note, that this intersection persists at some parameter region. However, the hyperchaotic Hénon-like attractor (as the classical Hénon attractor) is not pseudohyperbolic (robustly chaotic). It contains the saddle fixed point O with the two-dimensional unstable invariant manifold and (as we have an attractor) with such a saddle index $\rho = |\lambda_1\lambda_2|$, that $\rho < 1$. As was shown in [37–39], stable periodic orbits can appear in this case under arbitrarily small perturbations due to bifurcations of homoclinic tangencies.

2.2 Discrete Shilnikov attractor

As shown above, the period-doubling bifurcation can be the first step in the framework of onset of Hénon-like and hyperchaotic Hénon-like attractors. A natural question arises here. Which homoclinic attractors can appear if the first codimension-one bifurcation is a Neimark-Sacker bifurcation? The answer to this question was given in [31] (see also [26], and [27]) where a scenario for the appearance of the so-called *discrete Shilnikov attractor* containing a saddle-focus fixed point of (1,2)-type was proposed. This scenario goes back to the paper by Shilnikov [75] where a similar scenario was proposed for one-parameter families of three-dimensional systems of differential equations. Since this scenario plays an important role in the development of hyperchaos [23], let us briefly describe it.

2.2.1 General outline of the scenario of discrete Shilnikov attractor appearance

Suppose that at $\varepsilon < \varepsilon_1$ the fixed point O is stable but focal (a pair of its multipliers is complex-conjugate), see Fig. 6a. At $\varepsilon = \varepsilon_1$ it undergoes the supercritical Neimark-Sacker bifurcation. As a result, this fixed point becomes a saddle-focus of (1,2)-type, and a stable invariant curve L is born in its neighborhood, see Fig. 6b. Note that after the birth, this curve is of a nodal type: the two-dimensional unstable invariant manifold $W^u(O)$ is a disc with an edge on L. Then, we suppose that at $\varepsilon = \varepsilon_2$ the stable curve becomes focal, and, as a result, $W^u(O)$ starts to wind on it forming the so-called "Shilnikov whirlpool", see Fig. 6c. All orbits from the absorbing domain $D_a(O)$ (except the stable separatrix $W^{s-}(O)$) are drawn in by this whirlpool. With further increase in ε, the size of the whirlpool is increased, and finally, at $\varepsilon = \varepsilon_3$, the stable separatrix $W^{s+}(O)$ touches $W^u(O)$. As a result, at some interval $\varepsilon_3 < \varepsilon < \varepsilon_4$, the fixed point O has a transversal homoclinic structure. By Smale and Shilnikov [73, 78], in the neighborhood of the transversal intersection $W^u(O) \cap W^{s+}(O)$ there exist countably many periodic orbits of the same type as the fixed point O which is the saddle-focus of (1,2)-type.

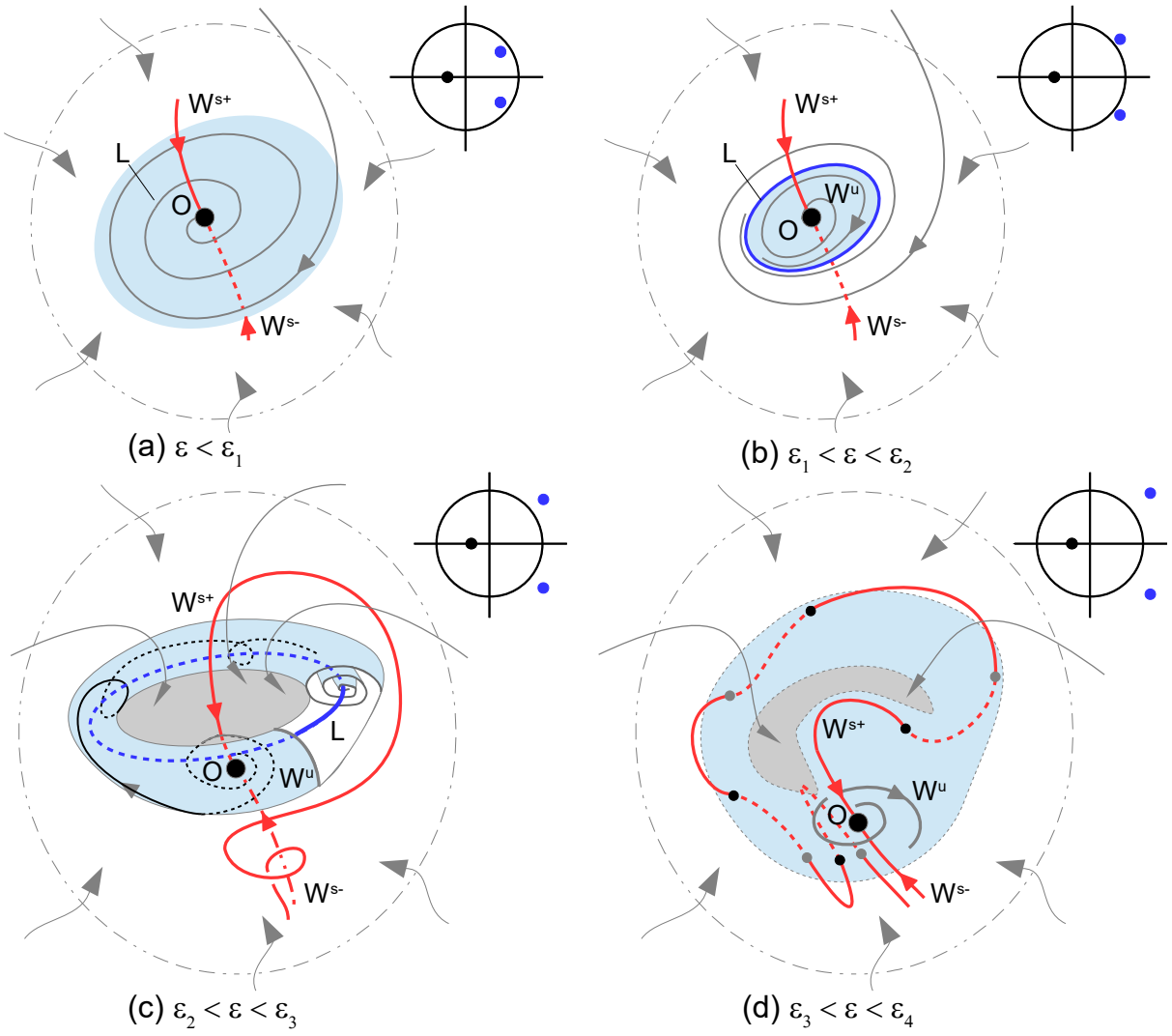

Figure 6: Onset of the discrete Shilnikov attractor containing the saddle-focus point O of (1,2)-type.

If the stable invariant curve L breaks down (by Afraimovich-Shilnikov [1] or due to some other scenario [49, 88–90]) giving chaotic attractor, then, on some subinterval inside $\varepsilon \in (\varepsilon_3, \varepsilon_4)$, this attractor can contain the fixed point O together with the nontrivial hyperbolic set of (1,2)-type. Therefore, this discrete Shilnikov attractor can be hyperchaotic.

Remark 2 *In the framework of the described scenario we suppose that the fixed point O undergoes the supercritical Neimark-Sacker bifurcation. However, it can undergo the subcritical Neimark-Sacker bifurcation, i.e., the point O can sharply lose the stability due to the merger with a saddle invariant curve existing in a neighborhood of O. In this case, a discrete Shilnikov attractor can appear suddenly. A similar scenario (but for a three-dimensional system of differential equations) was observed e.g. in [51].*

2.2.2 Detailed scenarios for hyperchaotic and flow-like discrete Shilnikov attractors appearance

Here we describe specific sequences of bifurcations responsible for the chaotization of the invariant curve L (Fig. 7a) and leading to the appearance of (i) hyperchaotic and (ii) flow-like strange attractors on the base of L. Suppose that, before the destruction, the invariant curve becomes resonant: a pair of stable and saddle period-q orbits O_q and S_q appears on it as a result of the saddle-node bifurcation. In this case, the curve L is formed by the the closure of the unstable one-dimensional invariant manifold of S_q, see Fig. 7b. Note that the stable two-dimensional invariant manifold of S_q forms the boundary of the absorbing domain for the stable point O_q or attractors emerging from it according to one of the two following scenarios.

1. The point O_q undergoes the supercritical period-doubling bifurcation after which it becomes the saddle of (2,1)-type and a stable period-$2q$ orbit O_{2q} is born in its neighborhood, see Fig. 7c, i.e., in this case we have a hypothetical possibility to obtain the hyperchaotic Hénon-like attractor on the base of O_q via the scenario described in Sec. 2.1.3. However, during this scenario, the cascade of period-doubling bifurcations of the stable point O_q can be interrupted at some moment by a Neimark-Sacker bifurcation occurring with some period-$2^i q$ orbit after which this periodic orbit gets the two-dimensional unstable manifold, and a stable $2^i q$-component invariant curve is born. In its turn, this curve before the destruction becomes resonant. Then, the stable resonant orbit bifurcates according to one of the two considered scenarios, and so on.

2. The point O_q undergoes the supercritical Neimark-Sacker bifurcation after which it becomes the saddle-focus of (1,2)-type and a stable q-component invariant curve L_q is born in its neighborhood, see Fig. 7d, i.e., here we have the possibility to obtain the hyperchaotic Shilnikov attractor on the base of O_q. The curve L_q before the destruction becomes resonant. Then, the stable resonant orbit bifurcates according to one of the two considered scenarios, and so on.

Concerning the resonant saddle orbit S_q, as well as other saddles arising in the framework of the described above scenarios, all they undergo cascades of period-doubling bifurcations resulting in the nontrivial hyperbolic sets of (1,2)-type (the same as with the saddle fixed point in the framework of the scenario described in Sec. 2.1.3). We denote such a hyperbolic set developed from the S_q-orbit $\mathrm{SH}_q(1,2)$. Touching the one-dimensional stable

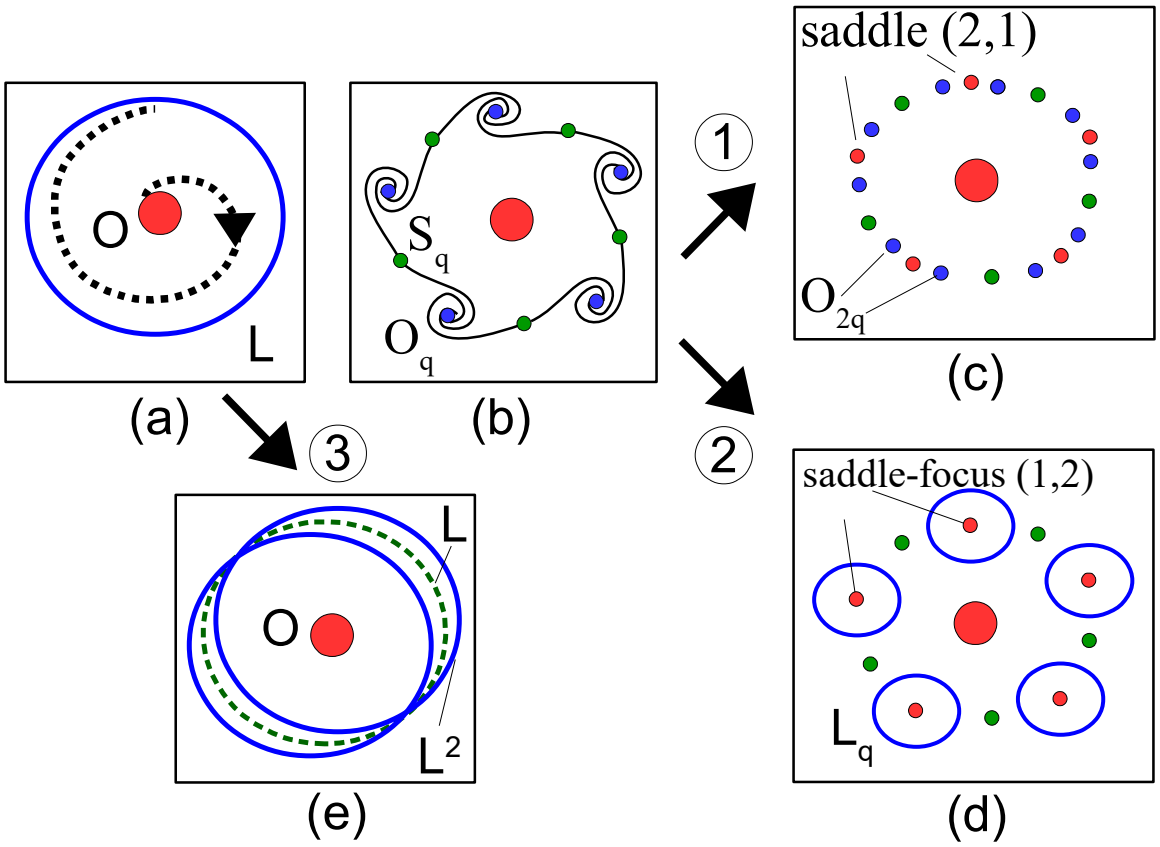

Figure 7: Schematic representation of two possible mechanisms of the destruction of the invariant curve L: (a) L is a nonresonant (ergodic) invariant curve; (b) L is a resonant curve (a pair of stable and saddle period-q orbits O_q and S_q appears on it via the saddle-node bifurcation); (c) O_q undergoes the supercritical period-doubling bifurcation (d) O_q undergoes the supercritical Neimark-Sacker bifurcation; (e) L undergoes a period-doubling (length-doubling) bifurcation.

manifolds of $\mathrm{SH}_q(1,2)$, the attractor emerging from O_q undergoes crisis and collides into a one-component attractor containing $\mathrm{SH}_q(1,2)$.

3. Note that before becoming resonant the curve L can go through a long sequence of period-doubling (length-doubling) bifurcations. After each such bifurcation the corresponding invariant curve becomes saddle, and a stable double-round invariant curve appears in its neighborhood (Fig. 7e). Such transition to chaotic attractors (including Shilnikov ones), is observed quite often (see e.g. [2, 3, 12, 14, 15, 42, 47, 80]) and can lead to the birth of the so-called flow-like chaotic attractor possessing one positive and one zero (indistinguishable from zero in numerical experiments) Lyapunov exponents (strange attractors with two zero Lyapunov exponents in the case of systems of differential equations). In Sec. 6 we demonstrate and study this phenomenon for the map (1).

3 Three-dimensional Mirá map: main bifurcations and dynamical regimes

In this section we study main bifurcations and discuss some interesting dynamical regimes in the three-dimensional Mirá map (1). Recall, that this map has a constant Jacobian, $J = B$. Various types of attractors are possible only when the map is dissipative, i.e., when $|B| < 1$. In this paper we consider only orientation-preserving case, when B is positive ($0 < B < 1$).

The map (1) has up to two fixed points $O_+(x_+, y_+, z_+)$ and $O_-(x_-, y_-, z_-)$ with coordinates

$$x_\pm = y_\pm = z_\pm = \frac{M_2 + B - 1}{2} \pm \sqrt{\frac{(1 - B - M_2)^2}{4} + M_1}. \tag{2}$$

As one can see, these points exist only when the root expression is non-negative. Points $O_\pm$ are born via the saddle-node (tangent) bifurcation (when one multiplier is equal to 1) occurring on the surface

$$\mathrm{SN} : M_1 = -\frac{(1 - B - M_2)^2}{4}. \tag{3}$$

A period-doubling bifurcation occurs when a multiplier is equal to -1 on the surface

$$\mathrm{PD} : M_1 = \frac{3(B + M_2)^2 + 2(B + M_2) - 1}{4}. \tag{4}$$

The third codimension-one bifurcation appears when a pair of multipliers becomes equal to $e^{\pm i\phi}, \phi \in (0, \pi)$ and $\phi \neq \{\pi/2, 2\pi/3\}$. This is a Neimark-Sacker bifurcation. It occurs on the surface

$$\mathrm{NS} : M_1 = \frac{(2 - M_2 - B + M_2 B - B^2)^2 - (1 - B - M_2)^2}{4}, \quad |M_2 - B| < 2. \tag{5}$$

Note that the relations (3)-(5) define in the three-dimensional parameter space (M_1, M_2, B) the region of stability of the point O_+. Figure 8 shows several slices of this space for various values of the parameter B. In this figure, the region of stability for O_+ is colored in blue, let us explain its boundaries.

The curves SN and PD are tangent at the codimension-two point *ff* corresponding to a *fold-flip bifurcation*. As known from the paper [53] (see also [25]), depending on coefficients of the corresponding normal form, this bifurcation can be of four possible types. Our studies show that here we observe the fourth case from [53]. The sketch for this bifurcation is shown in Fig. 8b. When crossing the SN-curve above the point *ff*, the stable fixed point O_+ is born together with the saddle O_-. The point O_- undergoes a period-doubling bifurcation on the curve PD above *ff*. As a result this point becomes saddle of type (1,2)-type and a period-2 saddle orbit of type (2,1) is born in its neighborhood. This period-2 orbit merges with the stable fixed point O_+ on the bottom piece of the PD-curve (below *ff*), after which the point O_+ becomes saddle of (2,1)-type. Finally, the saddle points O_+ and O_- merges on the bottom piece of the SN-curve and both disappear to the left of this curve.

In Figure 8 we also plot the region SH(1,2) inside which the nonwandering set of the map (1) is a hyperchaotic hyperbolic set consisting of saddle periodic orbits of (1,2)-type. We also call this set Smale horseshoe of (1,2)-type. According to the theorem by

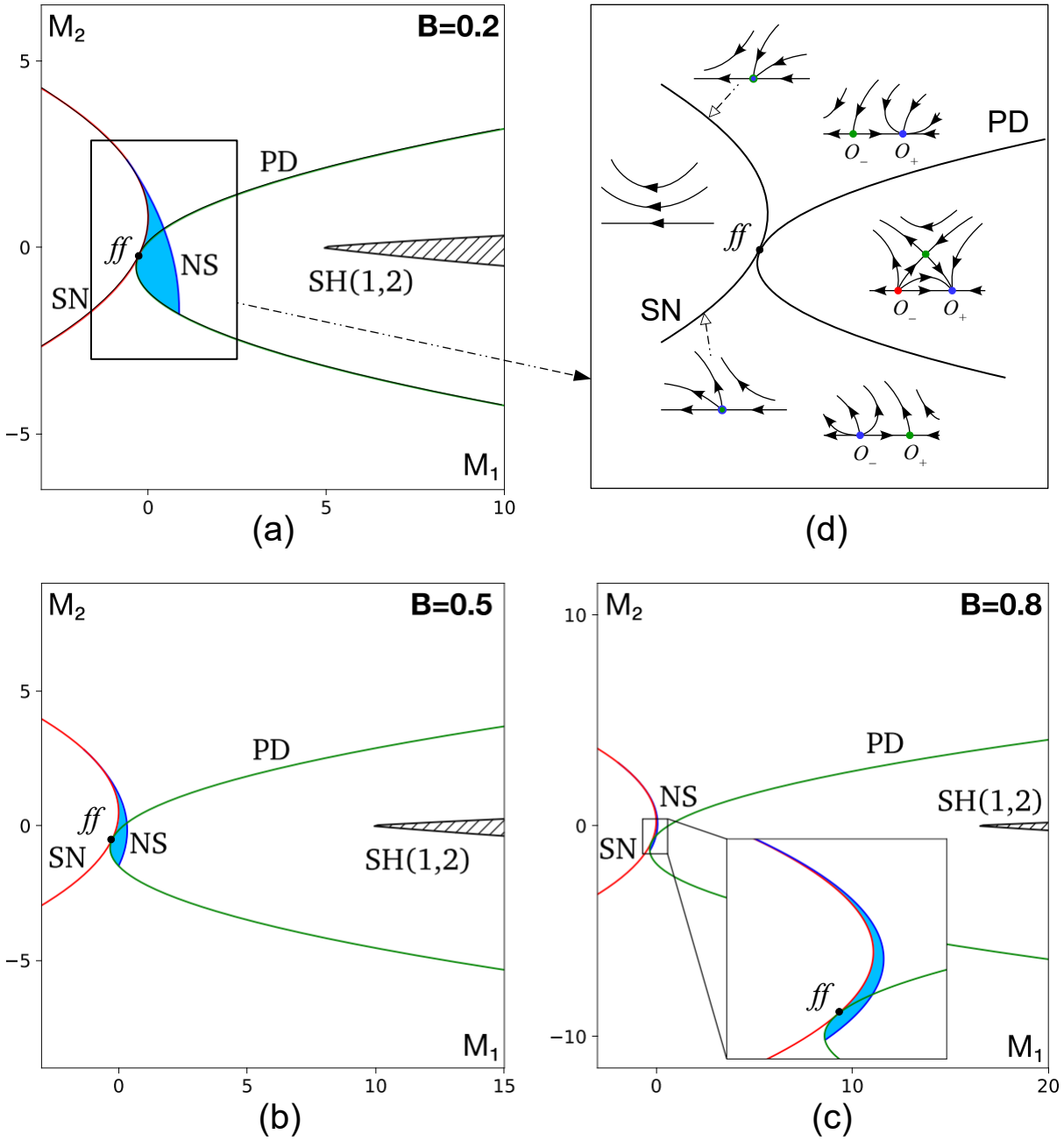

Figure 8: Some bifurcation curves for the map (1) for various values of parameter B: (a) $B = 0.2$, (b) $B = 0.5$, (c) $B = 0.8$. SN, PD, and NS are the saddle-node, period-doubling, and Neimark-Sacker bifurcation curves. The region of stability of the point O_+ is colored in blue. The region SH(1,2) corresponds to the existence of a nontrivial hyperbolic subset of (1,2)-type. (d) Sketch of the bifurcation diagram near the fold-flip bifurcation point *ff*. Here, the behavior of orbits on the corresponding center 2D manifold is shown; this invariant manifold is asymptotically stable in our case.

Gonchenko and Li (th. 2 in [29]), this region is bounded by the surface

$$M_1 = \left(\tilde{\rho} + \sqrt{\tilde{\rho}^2 + \frac{1}{4}}\right)^2 - (1 - M_2 - B)\left(\tilde{\rho} + \sqrt{\tilde{\rho}^2 + \frac{1}{4}}\right),$$

where

$$\tilde{\rho} = \frac{3 + 5(|B| + |M_2|)}{3 + 4(|B| + |M_2|)}(1 + |B| + |M_2|).$$

In this paper we study evolution of attractors along pathways from the region of stability of the fixed point O_+ towards the region SH(1,2).

As shown below, all interesting dynamical regimes in the map (1) for $0 < B < 1$ are associated with bifurcations of the fixed point O_+. Thus, it is convenient to shift this point to the origin which gives the following representation for the map (1)

$$\begin{cases} \bar{x} = y \\ \bar{y} = z \\ \bar{z} = Bx + Cy + Az - y^2. \end{cases} \tag{6}$$

The main difference between the maps (1) and (6) is that in the last map both fixed points O_+ and O_- always exist. The point O_+ becomes stable here under a transcritical saddle-node bifurcation (but note via the saddle-node bifurcations as for the map (1)) occuring on the plane

$$\mathrm{TR} : C = 1 - A - B. \tag{7}$$

Other boundaries of stability of this point are determined by a period-doubling bifurcation which occurs on the plane

$$\mathrm{PD}_1 : C = 1 + A + B \tag{8}$$

and by a Neimark-Sacker bifurcation occurring on the surface

$$\mathrm{NS}_1 : C = B^2 - AB - 1, \quad -2 < A - B < 2, \tag{9}$$

see the bifurcation diagram for $B = 0.5$ in Figure 9. Respectively, the relations (7)–(9) define in the three-dimensional parameter space (A, B, C) the region of stability of the fixed point O_+ bounded by the transcritical saddle-node (TR), period-doubling (PD_1), and Neimark-Sacker (NS_1) bifurcations.

In Figure 10 we show diagrams of Lyapunov exponents $\Lambda_1 \geq \Lambda_2 > \Lambda_3$ (Lyapunov diagrams) for various values of the Jacobian B ($B \in \{0.1, 0.3, 0.5, 0.7\}$).[6] For calculation of Lyapunov exponents we take an orbit on an attractor and estimate the exponents along its 10^6 iterations using the standard scheme [11]. Depending on values of LE, we use the following color coding: blue – for periodic orbits ($\Lambda_1 < 0$), green – for quasiperiodic regimes ($\Lambda_1 = 0, \Lambda_2 < 0$), yellow – for chaotic attractors ($\Lambda_1 > 0, \Lambda_2 < 0$), gray – for flow-like chaotic attractors ($\Lambda_1 > 0, |\Lambda_2| < 0.002$) and red – for hyperchaotic attractors ($\Lambda_1 > 0, \Lambda_2 > 0$).

Phase portraits of various attractors are shown in Figure 11. In Fig. 11a we demonstrate the stable invariant curve which appears after the supercritical Neimark-Sacker bifurcation of the fixed point O_+; in Fig. 11b – the stable period-4 orbit which emerges as a resonance on this curve; in Fig. 11c – the four-component Hénon-like attractor; in Fig. 11d – the hyperchaotic Hénon-like attractor on the base of period-4 saddle orbit, in Fig. 11e – the hyperchaotic four-component Shilnikov attractor; and in Fig. 11f – the hyperchaotic Shilnikov attractor containing the fixed point O_+.

[6] On these Lyapunov diagrams we plot only regimes associated with the fixed point O_+. Above the curve TR, the point O_- becomes stable via the transcritical saddle-node bifurcation (this point is swapped by the stability with O_+). However, we do not color the corresponding part of (A, C)-parameter plane.

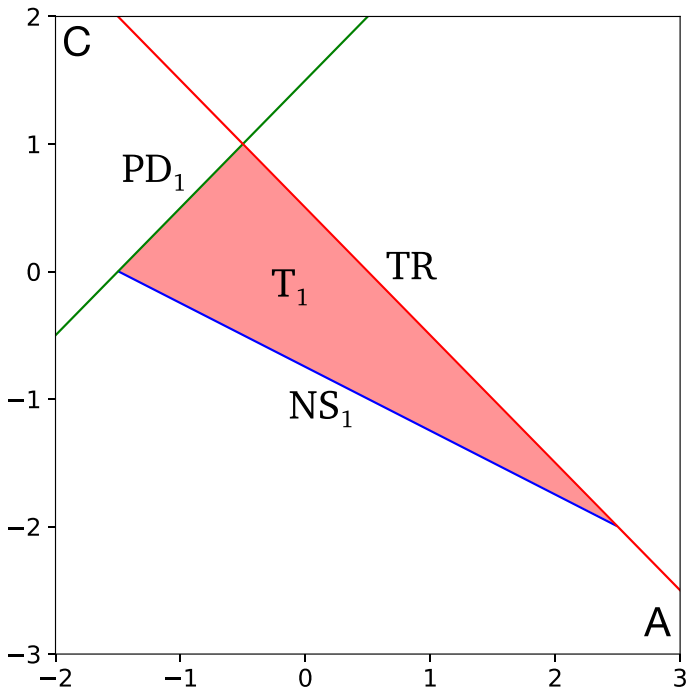

Figure 9: Some bifurcation curves of the map (6), $B = 0.5$. The curves TR, PD_1, and NS_1 correspond to the transcritical saddle-node, period-doubling, and supercritical Neimark-Sacker bifurcations. The region of stability of the point O_+ is colored in pink.

As one can see in Fig. 10, hyperchaotic attractors occupy large regions under the NS_1-curve of the supercritical Neimark-Sacker bifurcation. After this bifurcation, the point O_+ becomes saddle-focus of (1,2)-type and a stable invariant curve L is born in its neighborhood, see e.g. Fig. 11a. Depending on the rotation number ρ_N, this curve can be resonant (if ρ_N is rational, i.e., $\rho_N = p/q$) or ergodic (if ρ_N is irrational). In the parameter plane, regions corresponding to the stable ergodic curve alternate with the Arnold tongues originating from the curve of the Neimark-Sacker bifurcation where $\rho_N = p/q$. Inside the Arnold tongues (close enough to the curve NS_1) the stable invariant curve is resonant, see e.g. Fig. 11b. It is formed by the closure of the unstable invariant manifold of the period-q saddle orbit emerging together with the stable one on the boundaries of the corresponding Arnold tongue.

The largest tongues correspond to the resonances with small q. Among them, the so-called strong resonances 1:3 and 1:4 are the most interesting and important. The tongue corresponding to the 1:3 resonance originates from the point $(A, C) = (B - 1, B - 1)$. It gives quite thin regions with stable dynamics, see Fig. 10. However, inside it the emergence of chaotic [26, 31] and, even, hyperchaotic attractors is possible, see more detail in Section 6. On the contrary, a tongue corresponding to the 1:4 resonance gives the largest area with stable dynamics. It originates from the point $(A, C) = (B, -1)$. The stable period-4 orbit inside this tongue can give rise to different types of chaotic and, even, hyperchaotic homoclinic attractors containing this orbit. If the period-4 orbit undergoes a period-doubling bifurcation, we can obtain Hénon-like attractors, see Fig. 11c, and, finally, hyperchaotic Hénon-like attractors, see Fig. 11d. If the period-4 orbit undergoes the supercritical Neimark-Sacker bifurcation, giving a four-component stable invariant curve,

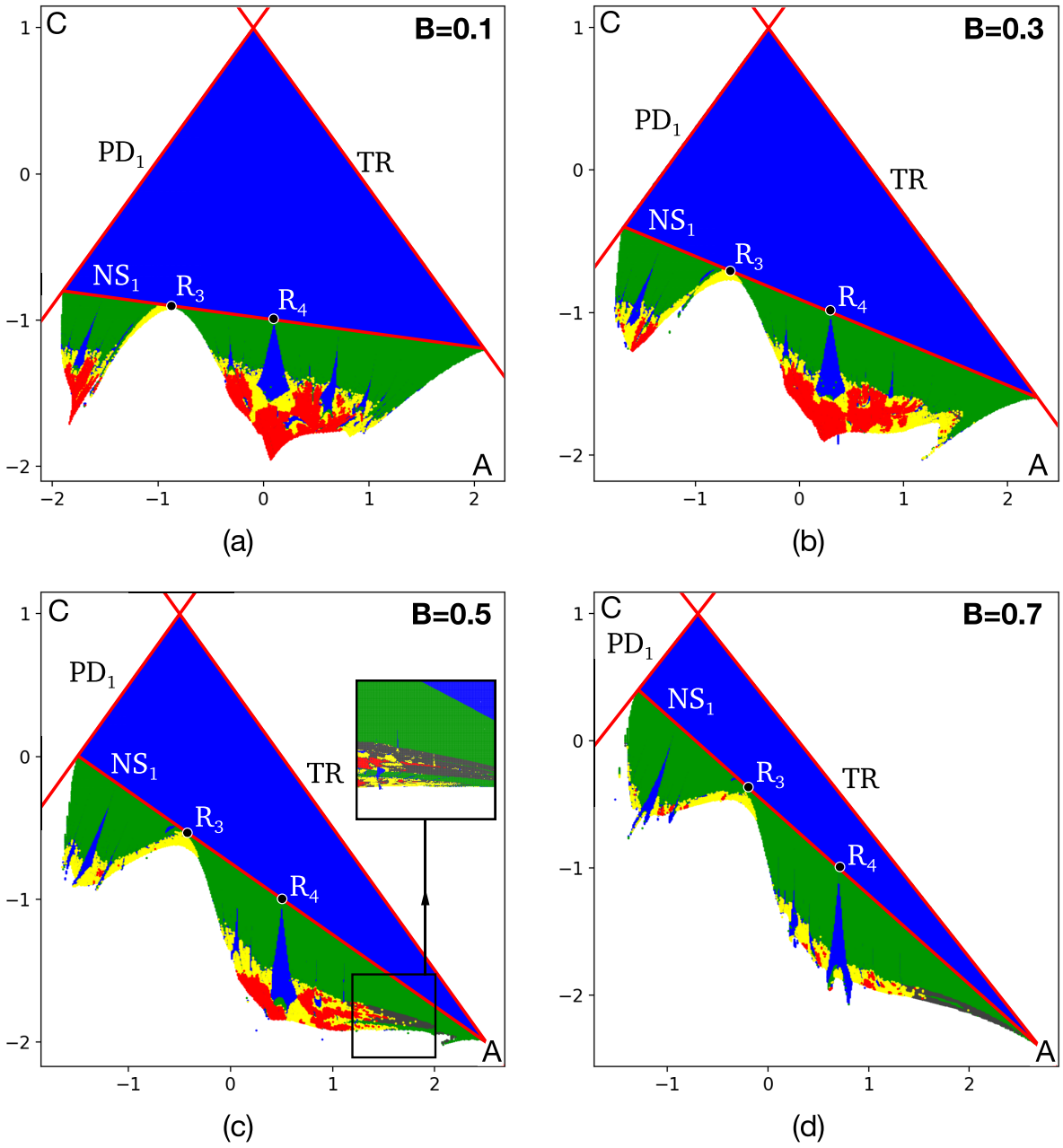

Figure 10: Lyapunov diagrams for the map (6) superimposed with the bifurcation curves TR, PD_1, and NS_1: (a) $B = 0.1$, (b) $B = 0.3$, (c) $B = 0.5$, and (d) $B = 0.7$. We use the following color coding: blue – periodic orbits ($\Lambda_1 < 0$); green – quasiperiodic regime ($\Lambda_1 = 0, \Lambda_2 < 0$); yellow – chaotic attractors with $\Lambda_1 > 0, \Lambda_2 < 0$; gray – "flow-like" chaotic attractors, when $\Lambda_1 > 0, \Lambda_2 \approx 0$; and red – hyperchaotic attractors with $\Lambda_1 > 0, \Lambda_2 > 0$.

we, then, can observe a four-component hyperchaotic Shilnikov attractor, see Fig. 11e, and, finally, hyperchaotic Shilnikov attractor containing the saddle-focus fixed point O_+. It is important to note that similar attractors and transitions to them are observed also in other Arnold tongues. In the framework of this paper, we study bifurcations associated only with the strong resonances 1:3 and 1:4. In particular, we show that hyperchaotic attractors on the base of the period-4 resonant orbit appear in accordance with the scenarios presented in Sec. 2.

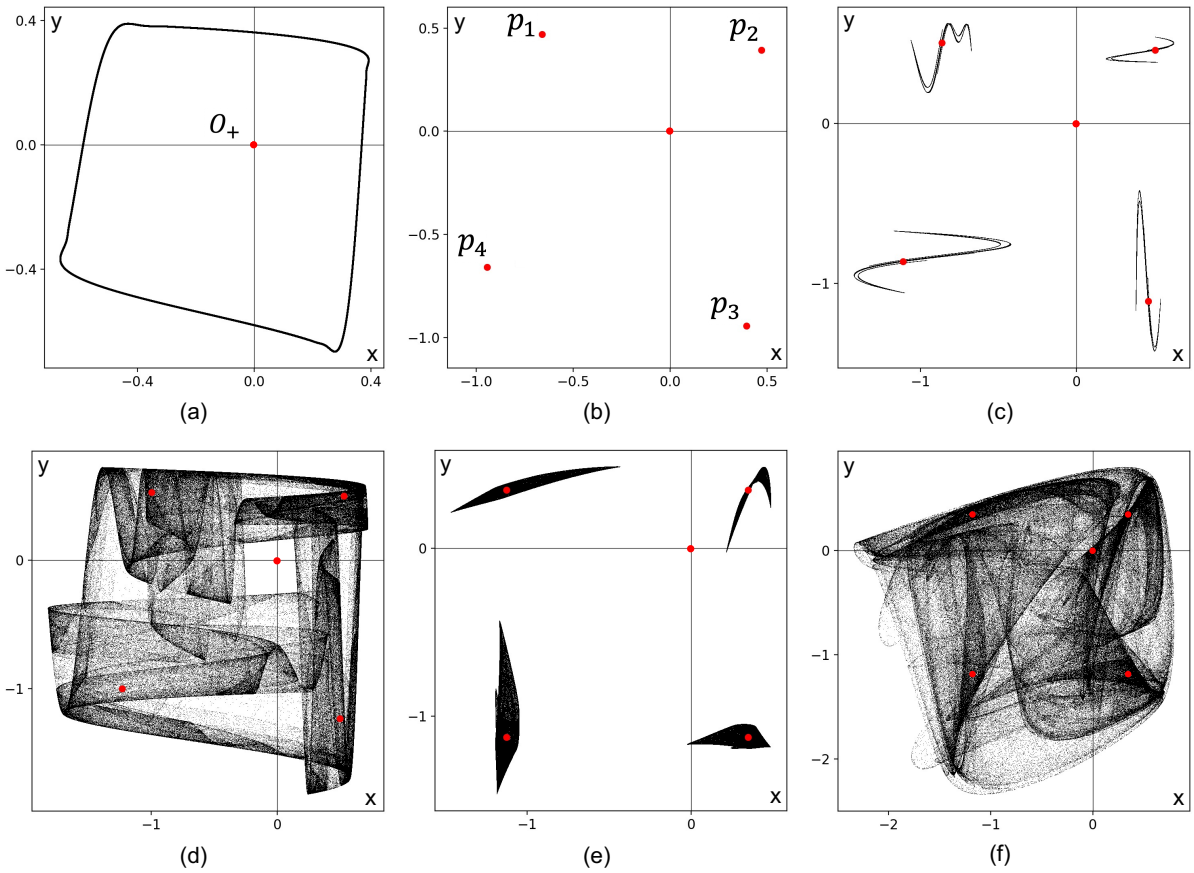

Figure 11: Phase portraits of various attractors of the map (6): (a) $A = 0, B = 0.1, C = -1.2$; (b) $A = 0, B = 0.1, C = -1.4$; (c) $A = 0, B = 0.1, C = -1.525$; (d) $A = 0, B = 0.1, C = -1.62$; (e) $A = 0.5, B = 0.5, C = -1.745$; (f) $A = 0.5, B = 0.5, C = -1.78$.

4 Hyperchaos in the map (6) via cascades of period-doubling bifurcations of periodic saddle orbits

In this section we study one of possible mechanisms for the appearance of hyperchaotic attractors in the map (6) with sufficiently small values of the Jacobian B.

4.1 The case $B = 0$ (numerical analysis of the 2D Mirá map)

We start with the case $B = 0$, when this map effectively coincides with the two-dimensional Mirá endomorphism. Lyapunov diagram near the 1:4 resonance, occurring at the point $(A, C) = (0, -1)$, and the corresponding part of the bifurcation diagram obtained with help of the MatContM package [40, 54, 64] are presented in Figure 12. One can see that hyperchaotic attractors can appear right below the region with stable periodic dynamics. Here, we explain the organization of bifurcation curves associated with the 1:4 resonance and the scenario for the appearance of hyperchaotic attractors in this case.

We denote the stable period-4 resonant orbit $P^4 = (p_1, p_2, p_3, p_4)$, and the corresponding saddle orbit (of (2,1)-type) $S^4 = (s_1, s_2, s_3, s_4)$. The left and right boundaries of the stability region for P^4 are formed by a pair of saddle-node bifurcation cures SN^4 originating from the codimension-two point R_4 where O_+ has a pair of multipliers $e^{\pm i\pi/2}$. The

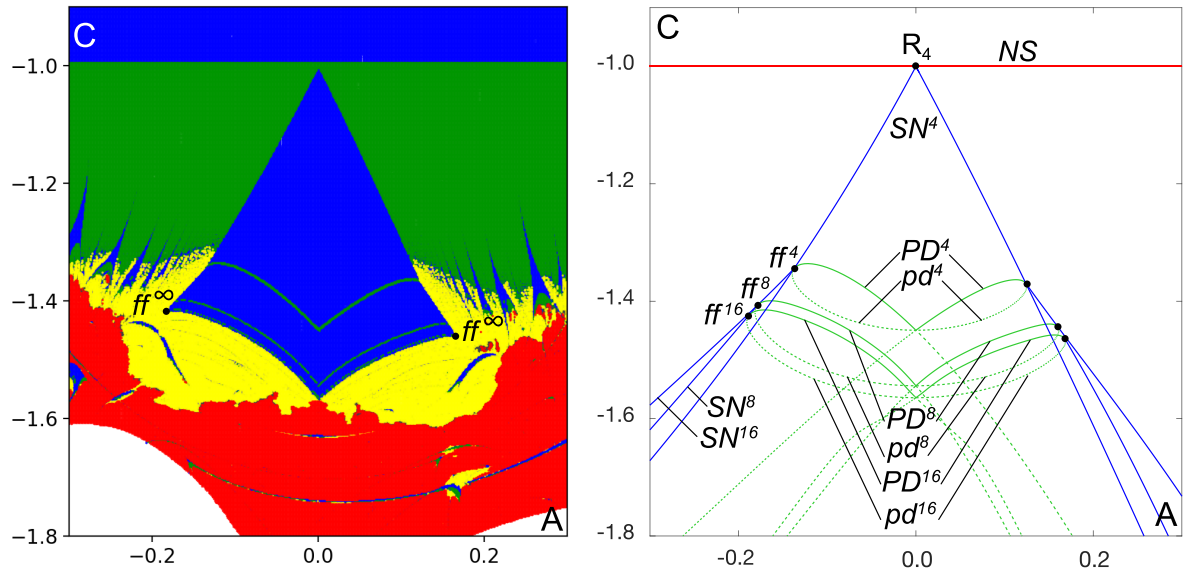

Figure 12: (a) Fragment of the Lyapunov diagram near the 1:4 resonance for the map (6) when $B = 0$; (b) the corresponding bifurcation diagram on which the saddle-node bifurcation curves SN^4, SN^8, and SN^{16} are colored in blue and the period-doubling bifurcation curves PD^4, PD^8, PD^{16}, pd^4, pd^8, and pd^{16} – in green (solid curves are used for bifurcations of stable orbits, while dashed – of saddle ones); the points ff^4, ff^8, and ff^{16} correspond to the fold-flip bifurcations; ff^∞ is a limit point for the fold-flip bifurcations.

bottom boundary consists of two curves PD^4 corresponding to the supercritical period-doubling bifurcation of P^4. The left (right) curve PD^4 is tangent to the left (right) curve SN^4 at a fold-flip bifurcation point ff^4, where P^4 has a pair of multipliers $(+1, -1)$. The same as for the fixed point of the map (1), here we observe the fourth case of bifurcation unfolding from Ref. [53] (see Fig. 8d). Namely, above this point, on the curves PD^4, the period-doubling bifurcation occurs with the stable periodic orbit P^4, while below this point, on the curves pd^4, period-doubling bifurcation occurs with the saddle period-4 orbit S^4. Respectively, the period-doubling bifurcation transforms the stable orbit P^4 to the saddle of type (2,1) and the saddle orbit S^4 to the saddle of type (1,2). Further, we explain bifurcations associated only with the left fold-flip point ff^4, keeping in mind that the bifurcations at the right fold-flip point are the same.

Very close to the point ff^4, there is one more important codimension-two bifurcation, which significantly contributes to the organization of the bifurcation diagram. On the curve PD^4, we observe a point of the degenerate period-doubling bifurcation which gives rise to a saddle-node bifurcation curve SN^8. A pair of stable and saddle period-8 orbits P^8 and S^8 is born when crossing the upper part of this curve. The fragment of the upper boundary of the stability region for P^8 is formed by the curve PD^4. The bottom boundary of this region consists (as for the period-4 orbit P^4) of two pieces PD^8 corresponding to the supercritical period-doubling bifurcation. The same as for P^4, the period-doubling bifurcation curve PD^8 for P^8 is tangent to the curve SN^8 at the fold-flip bifurcation point ff^8. The bottom branch of this curve (pd^8) corresponds to the period-doubling bifurcation of the saddle orbit S^8. Close to the point ff^8, on the curve PD^8, we again observe the degenerate period-doubling bifurcation which gives rise to a saddle-node bifurcation curve SN^{16} and so on.

Numerical experiments show that an infinite sequence of the fold-flip points ff^4, ff^8,

$ff^{16}, \dots$ accumulates to some point ff^{∞} belonging to the boundary between periodic and chaotic dynamics, see Fig. 12a. This cascade of the fold-flip bifurcations gives rise to a pair of cascades of period-doubling bifurcations: the first – with the stable periodic orbit P^4 (on the curves PD^4, PD^8, $\mathrm{PD}^{16}, \dots$) and the second – with the saddle periodic orbit S^4 (on the curves pd^4, pd^8, $\mathrm{pd}^{16}, \dots$). In its turn, the saddle periodic orbits $P^4, P^8, \dots$ undergo again cascades of period-doubling bifurcations which transform them from the saddles of (2,1)-type to the saddles of (1,2)-type. The dashed lines PD^4, PD^8, $\mathrm{PD}^{16}, \dots$ correspond to the first period-doubling bifurcations along these cascades.

We note that the curves PD^4 and pd^4, PD^8 and pd^8, etc., have additional common codimension-two points. At each such point the corresponding periodic orbit has the pair of multipliers $(-1, -1)$. All these points belong to the line $(B = 0, A = 0)$. When passing through them downward, both stable $P^4, P^8, \dots$ and saddle $S^4, S^8, \dots$ periodic orbits become saddles of type (1,2) simultaneously. The cascade of these codimension-two bifurcations accumulates to the so-called "double Feigenbaum point" [52]. Hyperchaotic attractor along this pathway appears exactly right below the blue-colored region with periodic dynamics. This phenomenon has a simple explanation. When parameters A and B vanish[7] the two-dimensional Mirá endomorphism can be rewritten as a pair of uncoupled identical parabola maps $\bar{u} = 1 - cu^2, \bar{v} = 1 - cv^2$, where hyperchaotic attractors appear right after the "last" period-doubling bifurcation occurring at $c \approx 1.401155$ [56].

Similar phenomena of the organization of bifurcation curves associated with the 1:4 resonance were previously found in several works. In Ref. [41], the authors studied the same unfolding of the fold-flip bifurcation of the period-4 orbit and the self-intersection of the corresponding period-doubling bifurcation curve in the duopoly model of Kopel [50]. These results were extended in the recent book [55] where bifurcations of the period-8 and period-16 orbits in this duopoly model were also studied. In Ref. [24] the same unfolding of the fold-flip bifurcation was found in a predator-prey map. Our studies extend these results to explain mechanisms of the appearance of hyperchaotic attractors.

4.2 The case $B = 0.1$ (3D Mirá map with small Jacobian)

Now we fix $B = 0.1$. Lyapunov diagram for this case is presented in Fig. 10a. Figure 13 shows a zoomed region of this diagram near the 1:4 resonance, and the corresponding bifurcation diagram. Let us, first, explain changes in the organization of the bifurcation curves associated with the 1:4 resonance and, then, study bifurcations along one-parameter pathways from the stable period-4 orbit P^4 to hyperchaotic attractors in the bottom part of this diagram.

As in the case $B = 0$, the left and right boundaries of the stability region for P^4 are formed by the pair of saddle-node bifurcation curves SN^4 originating from the codimension-two point R_4. However the bottom boundary of this region consists of three fragments: PD^4, NS^4, and again PD^4. The left and right fragments correspond to the same supercritical period-doubling bifurcation, and the small middle fragment corresponds to the supercritical Neimark-Sacker bifurcation. Here, again, the curves PD^4 are tangent to

[7] The evolution of chaotic dynamics with the transition from $A = 0$ and $B = 0$ to small values of these parameters can be rigorously traced using the anti-integrable limit approach [6, 60, 67, 68]. The applicability of this method for the analysis of 3D Hénon maps was shown in [43, 46]. We believe that this approach can be used to prove the existence of the Smale horseshoes of type (1,2) in the map (6) for sufficiently small values of parameters A and B.

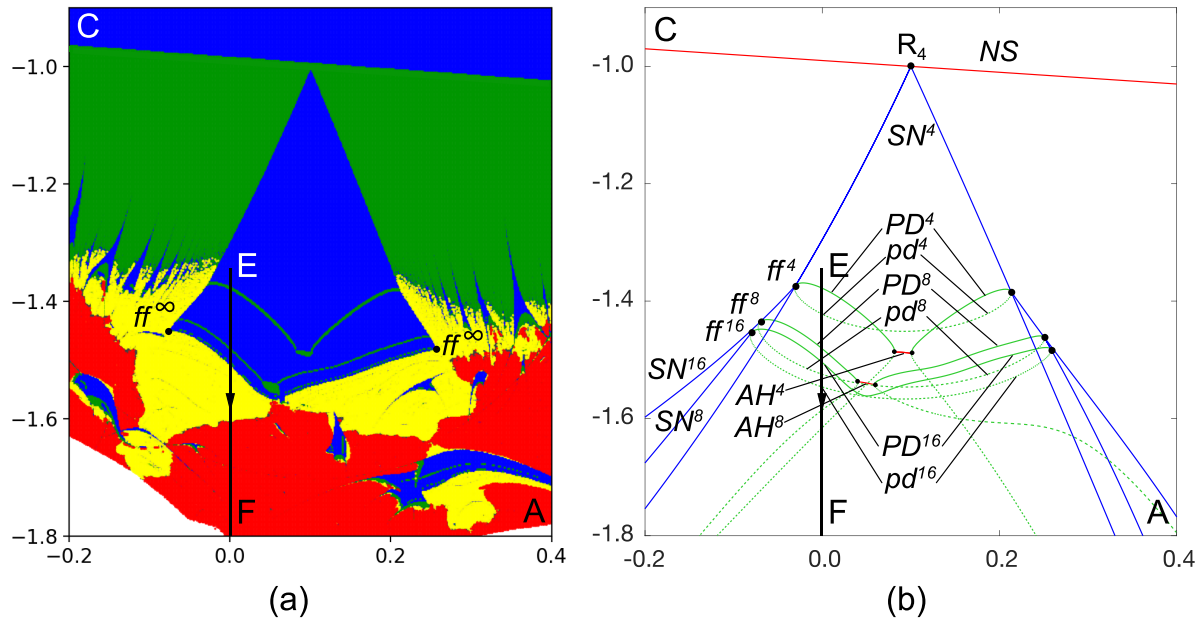

Figure 13: (a) Fragment of the Lyapunov diagram presented in Fig. 10a near the 1:4 resonance R_4; (b) the corresponding bifurcation diagram. Here we use the same denotations for bifurcation curves and points as in Fig. 12b, new red-colored curves NS^4 and NS^8 correspond to the Neimark-Sacker bifurcations.

the curves SN^4 at the fold-flip points ff^4, and the unfolding for these bifurcations is the same as in the case $B = 0$.

Near the point ff^4, on the curve PD^4, we found the degenerate period-doubling bifurcation point, which gives rise to the saddle-node bifurcation curve SN^8. As for $B = 0$, the stable period-8 orbit P^8 exists below the curve PD^4. The bottom boundary of this region consists (as for P^4) of three fragments: PD^8, NS^8, and again PD^8. The same as for P^4, for P^8 the period-doubling bifurcation curve PD^8 is tangent to the curve SN^8 at the fold-flip bifurcation point ff^8. On the upper branch of this period-doubling bifurcation curve we again observe the degenerate period-doubling bifurcation which gives rise to the saddle-node bifurcation curve SN^{16} and so on.

In addition to the points of the degenerate period-doubling bifurcations, here the type of period-doubling bifurcations along the curves PD^4, PD^8, ... is also changed at the 1:2-resonance points, where PD^4 intersects with NS^4, PD^8 intersects with NS^8, etc. As we show further, the length of curves corresponding to the Neimark-Sacker bifurcations NS^4, NS^8, ... is increased with increasing in parameter B.

4.2.1 One-parameter bifurcation analysis

Along pathways transverse to the lines PD^n and pd^n one can expect the implementation of the scenario presented in Section 2.1.3. Here we confirm it by analysing bifurcations along a one-parameter pathway EF with fixed $A = 0$ ($B = 0.1$, C is changed). The corresponding results are shown in Figure 14.

First, the stable orbit P^4 undergoes the cascade of period-doubling bifurcations, see phase portrait after the first two steps (slightly below the curve PD^{16}) in Fig. 14a. The orbit P^4 becomes saddle of (2,1)-type after the first period-doubling bifurcation. Then, with further decrease in C, the cascade of heteroclinic band-merging bifurcations occurs, and,

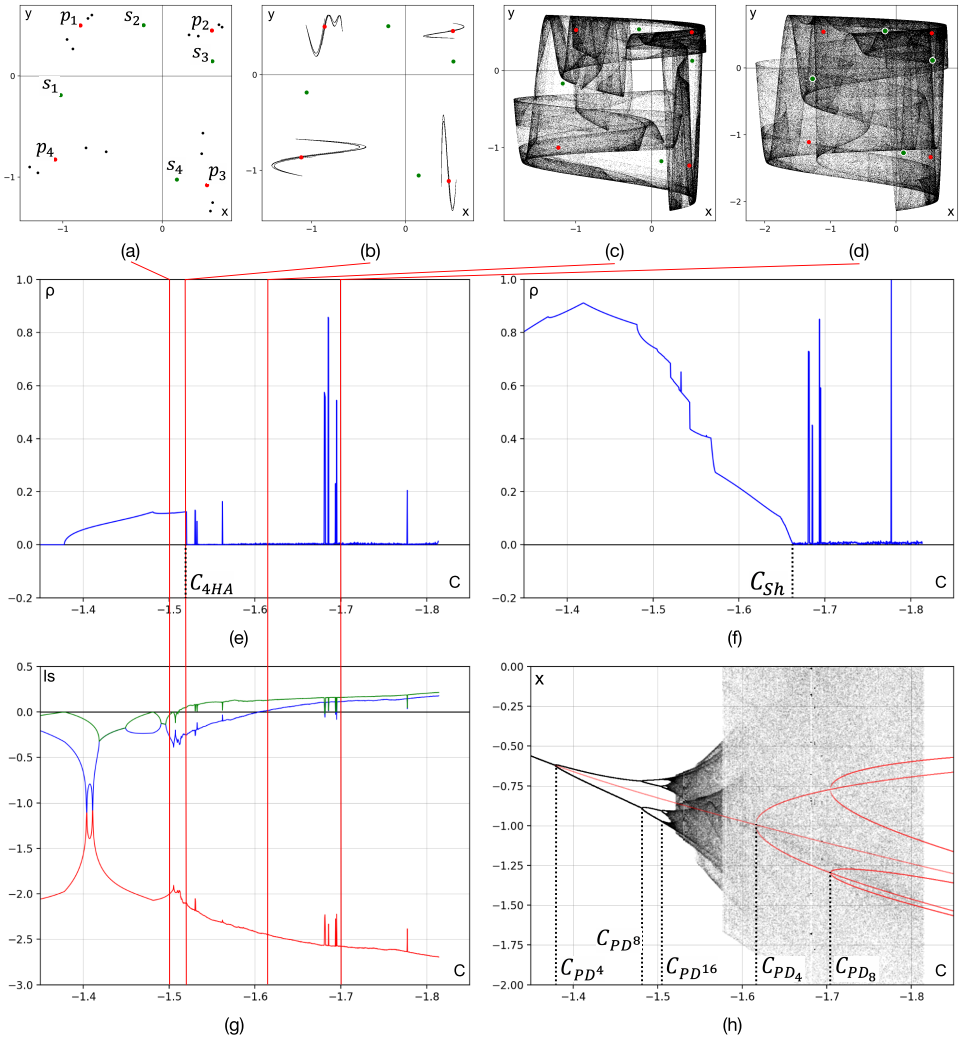

Figure 14: Graphs illustrating the onset of hyperchaotic attractors along the pathway EF: ($B = 0.1, A = 0$). (a)–(d) phase portraits of the attractors: (a) $C = -1.5$ – period-16 stable orbit after two steps in the cascade of period-doubling bifurcation of the stable period-4 orbit $P^4 : (p_1, p_2, p_3, p_4)$; (b) $C = -1.525$ – four-component Hénon-like attractor containing P^4 of (2,1)-type (LE: $\Lambda_1 = 0.073$, $\Lambda_2 = -2.156$, and $\Lambda_3 = -0.22$); (c) $C = -1.62$ – hyperchaotic Hénon-like attractor containing P^4 of (1,2)-type (LE: $\Lambda_1 = 0.132$, $\Lambda_2 = 0.027$, and $\Lambda_3 = -2.462$); (d) $C = -1.7$ – hyperchaotic Shilnikov attractor containing the saddle-focus fixed point O_+ of (1,2)-type (LE: $\Lambda_1 = 0.160$, $\Lambda_2 = 0.114$, and $\Lambda_3 = -2.577$). (e) The graph of the distance between the attractor and p_1; (f) the graph of distance between the attractor and O_+; (g) the graph of Lyapunov exponents Λ_1, Λ_2, and Λ_3 on parameter C; (h) bifurcation trees depicting dependency of the x-coordinate on parameter C for every fourth iteration of the map (in black color) and continuation of p_1 (in red color).

as a result, a four-component Hénon-like attractor containing P^4 appears, see Fig. 14b. The corresponding bifurcation tree is depicted in Fig. 14h. In Fig. 14e showing the graph of the distance between the attractor and p_1 component of P^4, one can see that the saddle orbit P^4 starts to belong to the attractor (which means the appearance of the Hénon-like attractor) at $C = C_{4HA} \approx -1.52$.

The next step in the framework of the hyperchaotic attractor development is a period-doubling bifurcation of the saddle orbit P^4 occurring on the curve PD_4 (at $C = C_{PD_4} \approx -1.616$). After this bifurcation, P^4 becomes saddle of (1,2)-type and a period-8 saddle orbit of (2,1)-type appears in its neighborhood, see the red-colored continuation tree

for the p_1 component of P^4 in Fig. 14h. As it can be seen in Figs. 14e and Fig. 14h, at $C < C_{PD_4}$ the point p_1 also belongs to the attractor. Moreover, as it is shown in the graph of Lyapunov exponents presented in Fig. 14g, the attractor becomes hyperchaotic near the mentioned above period-doubling bifurcation. The resulting hyperchaotic attractor at $C = -1.62$ is presented in Fig. 14c.

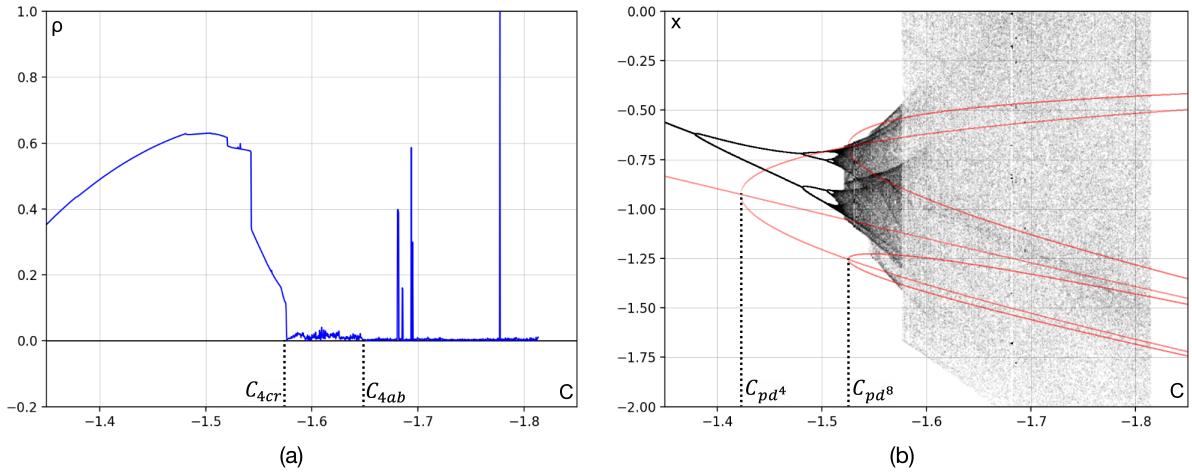

Figure 15: Diagrams illustrating bifurcations of the period-4 saddle orbit $S^4 = (s_1, s_2, s_3, s_4)$ which appears together with P^4 via the saddle-node bifurcation on the curve SN^4: (a) the graph of the distance between the attractor and s_1; (b) bifurcation tree depicting dependency of x-coordinate on parameter C for every fourth iteration of the map superimposed with the continuation tree for s_1.

Note that before the period-doubling bifurcation (at $C > C_{PD_4}$) with the saddle orbit P^4, the four-component Hénon-like attractor collides into the one-component attractor. It happens due to the boundary crisis: the unstable invariant manifold $W^u(P^4)$, forming the attractor, begins to intersect with the two-dimensional stable invariant manifold of the period-16 saddle orbit forming the boundary of its absorbing domain. (The corresponding heteroclinic bifurcation occurs at $C = C_{4cr} \approx -1.58$, see the jump of the distance between the attractor and s_1 in Fig. 15a). This period-16 saddle orbit appears after two successful period-doubling bifurcations (happened on the curves pd^4 and pd^8, see Fig. 13b) with the saddle orbit S^4 which, as was mentioned above, goes through the full cascade of period-doubling bifurcations (see also the red-colored tree in Fig. 15b). With a further decrease in C, at $C = C_{4ab} \approx -1.65$, the attractor absorbs the saddle orbit S^4 of type (1,2), see again Fig. 15a.

It is worth noting that the hyperchaotic attractor presented in Fig. 14c contains the orbits P^4 and S^4 but does not contain the fixed point O_+ which becomes a saddle-focus of (1,2)-type at $C < -0.99$. With a further decrease in C, the distance between the attractor and this fixed point decreases and, finally, at $C = C_{Sh} \approx -1.66$ it vanishes, see Fig. 14f. As a result, the hyperchaotic Shilnikov attractor appears, see Fig. 14d.

5 Hyperchaos in the map (6) via the appearance of multicomponent Shilnikov attractors

In this section we study scenarios for the appearance of hyperchaotic attractors in the map (6) with not very small values of the Jacobian B.

5.1 The case $B = 0.5$

Lyapunov diagram for $B = 0.5$ is presented in Fig. 10c. As in the previous case, hyperchaotic attractors appear here after the destruction of the stable invariant curve L. However, another mechanisms of the destruction of L is more typical in this case.

Figure 16 shows an enlarged fragment of the Lyapunov diagram near the 1:4 resonance and the corresponding part of the bifurcation diagram. Here we use the same denotations for bifurcation curves and periodic orbits as in Sec. 4.

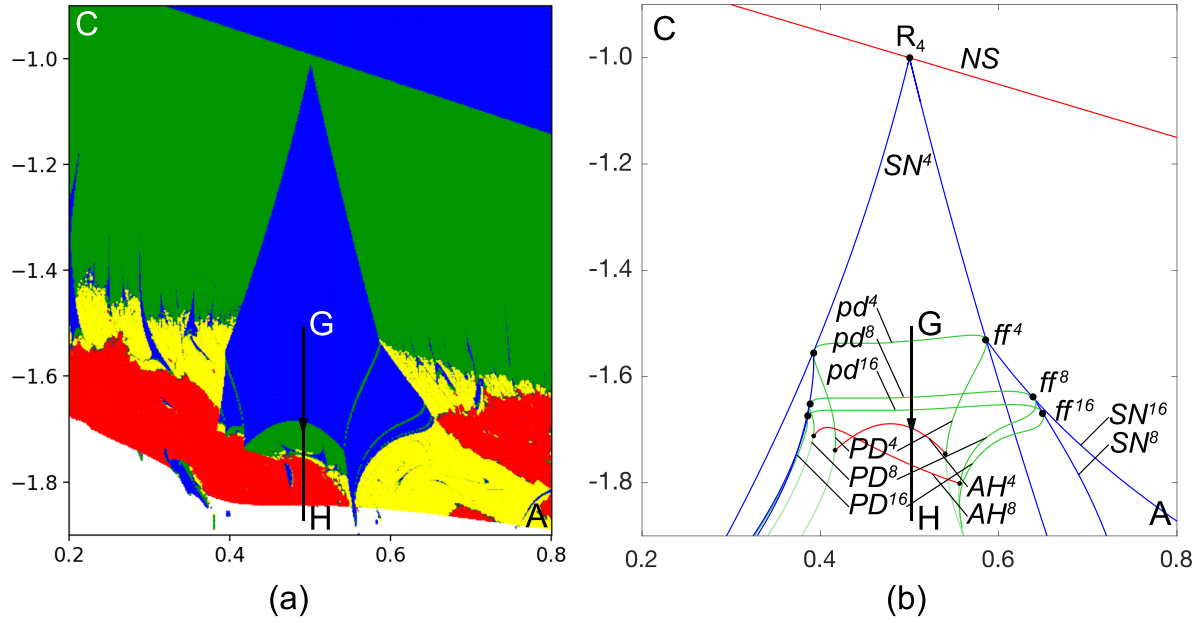

Figure 16: (a) $B = 0.5$. Fragment of the Lyapunov diagram near the 1:4 resonance R_4, and (b) the corresponding bifurcation diagram on which we use the same denotations for bifurcation curves and points as in Fig. 12b.

As in the previous case, here we observe the cascade of fold-flip bifurcations (ff^4, $ff^8, \dots$) which gives rise to the pair of cascades of period-doubling bifurcations of the stable period-4 orbit P^4 (the curves PD^4, $\mathrm{PD}^8, \dots$) and of the saddle period-4 orbit S^4 (the curves pd^4, $\mathrm{pd}^8 \dots$). The degenerate period-doubling bifurcations occurring on the curves PD^4, $\mathrm{PD}^8, \dots$ near the corresponding fold-flip points generate the cascade of the saddle-node bifurcation curves SN^4, $\mathrm{SN}^8, \dots$. The pair of period-$(4 \cdot 2^n)$ stable and saddle orbits appears with the intersection of each such curve.

However, unlike the case of small values of the Jacobian B, the curves pd^4, $\mathrm{pd}^8 \dots$ are located above the curves PD^4, $\mathrm{PD}^8, \dots$, compare Fig. 13b and Fig. 16b. A more detailed study of the transformation of bifurcation diagrams from the case of small values of B (in particular, starting from $B = 0$) to the case of non-small values of this parameter seems to be a very interesting problem for future research.

As in the case of small B, the stability region for the period-4 orbit P^4 is bounded from below by the period-doubling bifurcation curve PD^4, the Neimark-Sacker bifurcation curve NS^4, and again the period-doubling bifurcation curve PD^4. However, the fragment NS^4 is much wider here comparing with the case of small B. Moreover, the curves of period-doubling and Neimark-Sacker bifurcations are organized in such a way that typical pathways from the stable orbit P^4 to hyperchaotic attractors pass through one of the

Neimark-Sacker bifurcation curves, see Fig. 16.

5.1.1 One-parameter bifurcation analysis

Here we fix $A = 0.5$ (together with $B = 0.5$) and study bifurcations along a pathway GH from the stable period-4 orbit P^4 to hyperchaotic attractors decreasing parameter C. The results of corresponding one-parameter analysis are shown in Figure 17.

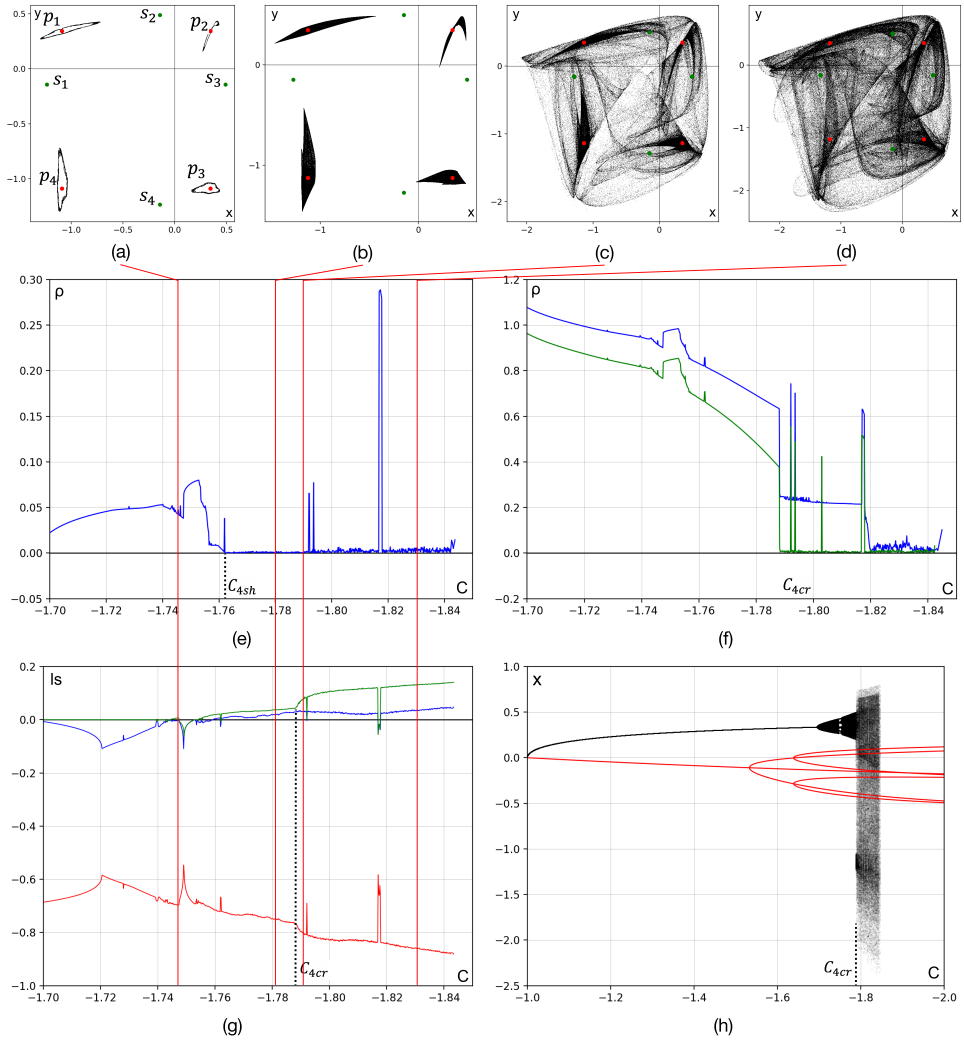

Figure 17: Graphs illustrating the onset of hyperchaotic attractors along the pathway GH: ($B = 0.5, A = 0.5$). (a)–(d) phase portraits of attractors: (a) $C = -1.745$ – four-component torus-chaos attractor; (b) $C = -1.78$ – four-component hyperchaotic Shilnikov attractor containing the saddle-focus period-4 orbit P^4 (LE: $\Lambda_1 = 0.036$, $\Lambda_2 = 0.0187$, and $\Lambda_3 = -0.748$); (c) $C = -1.79$ – four-component attractor transforms to the one-component attractor (LE: $\Lambda_1 = 0.072$, $\Lambda_2 = 0.0315$, and $\Lambda_3 = -0.797$); (d) $C = -1.83$ – hyperchaotic Shilnikov attractor containing the saddle-focus fixed point O_+ (LE: $\Lambda_1 = 0.131$, $\Lambda_2 = 0.0346$, and $\Lambda_3 = -0.858$). (e) the graph of distance between the attractor and the p_1-component of P^4. (f) the graphs of the distance between the attractor and O_+ (in blue color), and the attractor and the s_1-component of S^4 (in green color). (g) the graph of LE on parameter C. (h) bifurcation trees depicting dependency of x-coordinate on parameter C for every fourth iteration of the map (in black color) and continuation of s_1 (in red color).

Unlike the cases of small B (see Sec. 4), the stable period-4 orbit P^4 undergoes here the supercritical Neimark-Sacker bifurcation when crossing the curve NS^4. As a result,

the stable four-component invariant curve is born in the neighborhood of P^4 while this orbit becomes the saddle-focus of (1,2)-type. With decreasing C, this four-component curve breaks down and a four-component "torus-chaos" attractor (with only one positive Lyapunov exponent, see the graph of Lyapunov exponents in Fig. 17g) appears, see Fig. 17a.

Then, according to the scenario described in [23, 79] (see also Sec. 2.2), this torus-chaos attractor absorbs the saddle-focus orbit P^4 and, as a result, the four-component hyperchaotic Shilnikov attractor appears, Fig. 17b. This attractor is homoclinic, it contains P^4, its unstable invariant manifold W^u, and homoclinic points belonging to the intersection $W^u(P^4) \cap W^s(P^4)$. As it can be seen from Fig. 17e, depicting the distance between the attractor and p_4-component of P^4, the attractor starts to contain P^4 at $C = C_{4Sh} \approx -1.762$. Moreover, P^4 belongs to the attractor on a quite large interval of parameter C. Figure 18a depicting the phase portrait of the attractor and the stable one-dimensional manifold $W^s(P^4)$ shows that $W^u(P^4)$ and $W^s(P^4)$ intersect transversally. By Smale and Shilnikov [73, 78], the emergence of such an intersection implies a countable many saddle-focus orbits with two-dimensional unstable manifolds inside the attractor.

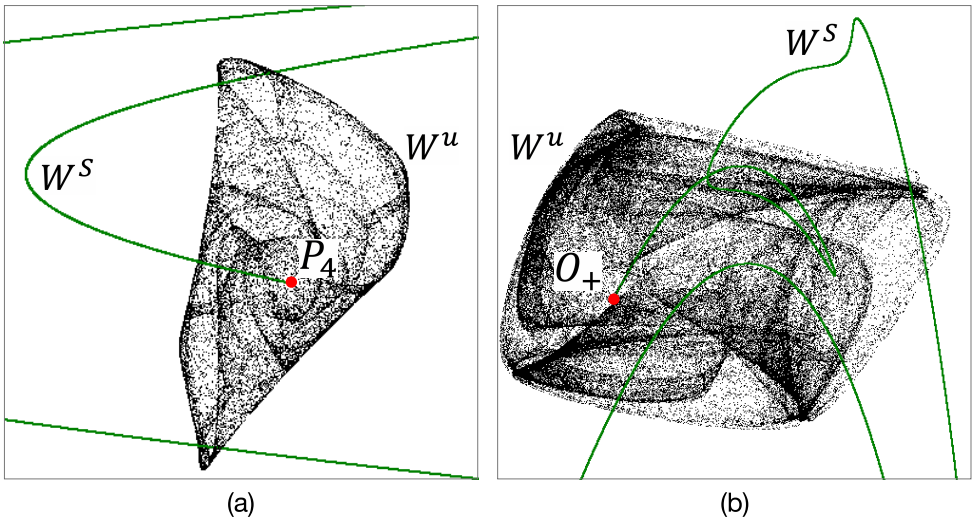

Figure 18: Phase portraits of (a) one component of the hyperchaotic four-component Shilnikov attractor presented in Fig. 17c, and (b) hyperchaotic Shilnikov attractor containing O_+ shown in Fig. 17d. Green-colored curve in both panels is the branch of the stable invariant manifold W^s that intersects with the unstable manifold W^u forming the attractor.

The onset of the four-component Shilnikov attractor is not the final step in the framework of the development of hyperchaotic dynamics along the pathway GH. With a further decrease in C (at $C = C_{4cr} \approx -1.789$), this attractor collides into the one-component attractor, see Fig. 17c. As in the case described in Sec. 4, this collision happens due to the boundary crisis, see the explosive growth of the attractor sizes in the bifurcation tree presented in Fig. 17h and the jump of the distance between the attractor and s_1-component of S^4 in Fig. 17f (green-colored graph). However, in this case, the period-4 saddle orbit S^4 undergoes before the crisis of the attractor a complete cascade of period-doubling bifurcations (on the curves pd^4, $\mathrm{pd}^4, \ldots$ in Fig. 16b), see a part of the continuation tree for the s_1-component of S^4 in Fig. 17h (red-colored graph). As a result, a non-attractive hyperbolic set with the two-dimensional unstable manifold appears on the base of this

orbit. At $C = C_{4cr}$, the four-component attractor touches the stable manifolds of this set and, at $C < C_{4cr}$, merges with it into the one-component attractor. Note that this collision is also clearly visible in the graph of Lyapunov exponents presented in Fig. 17g, where one can observe the jump of the second Lyapunov exponent (the so-called jump of hyperchaoticity [79]) at $C = C_{4cr}$ associated with this collision.

The one-component hyperchaotic attractor presented in Fig. 17c contains both periodic saddle orbits P^4 and S^4 which have the two-dimensional unstable manifold but does not contain the saddle-focus fixed point O_+. With a further decrease in C, the distance between the attractor and this point decreases and finally, at $C = C_{ab} \approx -1.820$, it vanishes, see the blue-colored graph in Fig. 17f. As a result, a hyperchaotic Shilnikov attractor containing the point O_+ appears, see Fig. 17d. It contains infinitely many saddle-focus, as well as saddle periodic orbits with the two-dimensional unstable manifolds. Figure 18b shows the transversal homoclinic structure for this attractor, additionally confirming the inclusion of O_+ to the attractor.

Further decrease in C leads to the destruction of the homoclinic Shilnikov attractor which happens via the boundary crisis: the unstable manifold $W^u(O_+)$ forming the attractor intersects with the stable two-dimensional manifold $W^s(O_-)$ bounding its absorbing domain.

We would like to underline that the similar transition to hyperchaos is observed also along other pathways from the stable fixed point O_+ to hyperchaotic attractors. Passing through other Arnold tongues, corresponding e.g. to a p/q-resonance, one can observe the transition from the stable period-q orbit to the Shilnikov attractor containing this orbit which becomes the saddle-focus of (1,2)-type after the corresponding Neimark-Sacker bifurcation. Then, the q-component Shilnikov attractor collides into the one-component attractor which, with a further decrease in C, can absorb the saddle-focus fixed point O_+ before the crisis.

However, it is not the case for the transition near the strong 1:3 resonance. We do not observe a stable period-3 orbit inside the corresponding tongue despite the possible existence (e.g. for $B = 0.7$) of hyperchaotic attractors below it, see Fig. 10d. The enlarged fragment of the corresponding Lyapunov diagram is presented in Figure 19a. Let us briefly describe main stages of the development of hyperchaotic attractors along a vertical pathway passing through $A = -0.44$. The stable invariant curve L deforms near the 1:3 resonance, see Fig. 19b. Then, a higher periodic resonance occurs inside the corresponding Arnold tongue, see Fig. 19c. With a further decrease in C, a multi-component invariant curve, appears from this periodic orbit under the supercritical Neimark-Sacker bifurcation. Soon, this curve breaks down giving torus-chaos attractor, see Fig. 19d. Finally, this strange attractor becomes hyperchaotic, see Fig. 19e.

6 Chaotic attractors with zero second Lyapunov exponent

In Sections 4 and 5 we have studied the appearance of homoclinic attractors in the map (6) for both cases of small and not very small values of the Jacobian B. In these cases the evolution of attractors is terminated via the boundary crisis. We have shown that, before this, the attractor can absorb the fixed point O_+ of the saddle-focus (1,2)-type, which gives the formal possibility for the attractor to become hyperchaotic.

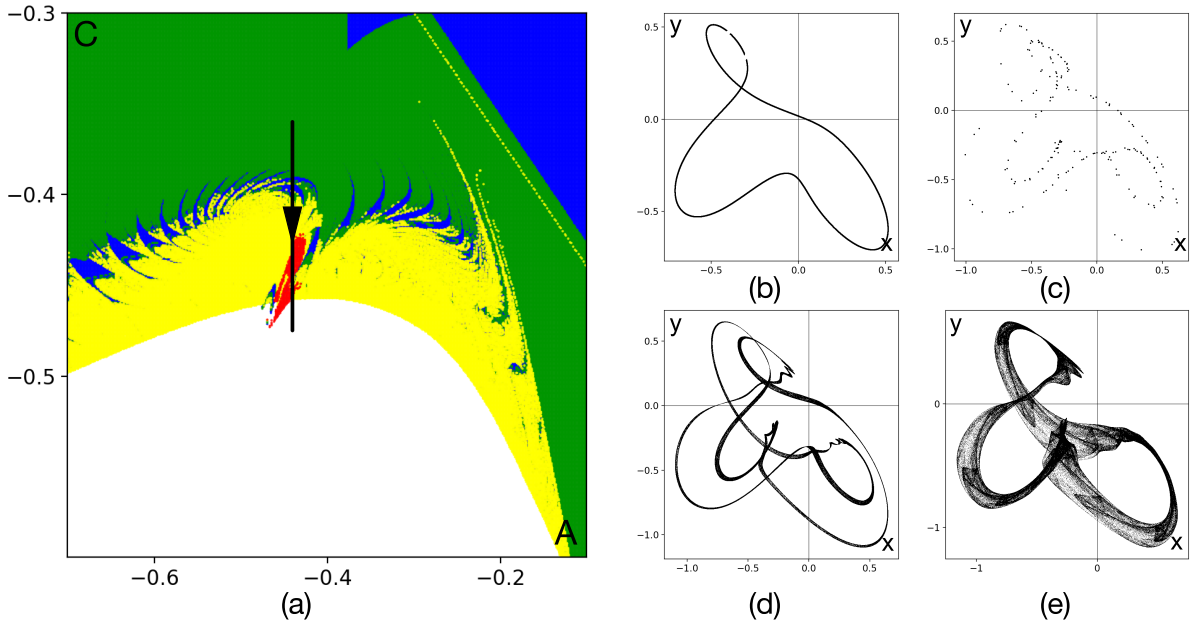

Figure 19: (a) Fragment of the Lyapunov diagram near the 1:3 resonance, $B = 0.7$. (b)–(e) Phase portraits of attractors along the pathway with fixed $A = -0.44$: (b) $C = -0.36$, the stable invariant curve L deforms near the 1:3 resonance; (c) long-period resonance appears inside the corresponding small Arnold tongue; (d) $C = -0.41$, torus-chaos attractor (LE: $\Lambda_1 = 0.017$, $\Lambda_2 = -0.011$, and $\Lambda_3 = -0.363$) (e) $C = -0.44$, hyperchaotic attractor (LE: $\Lambda_1 = 0.015$, $\Lambda_2 = 0.004$, and $\Lambda_3 = -0.376$).

However, bifurcations with chaotic attractors in the map under consideration do not always result in hyperchaos. In this section, we show that for sufficiently large values of the Jacobian $|B| < 1$ chaotic attractors (including Shilnikov ones) can be flow-like, i.e., their second Lyapunov exponent can be indistinguishable from zero in numerical experiments in quite large regions of the parameter space. This in itself is not a new phenomenon. Flow-like chaotic attractors were previously observed in the three-dimensional Hénon map [36], in the Lorenz-84 model [15], in some class of 3D diffeomorphisms of the torus [14], in nonholonomic models of Celtic stone [28] and Chaplygin top [12], in models of identical globally coupled oscillators [42] and in other systems. In this section we give an explanation for this phenomenon suitable for the map (6) as well as for many other cases.

Figure 20 shows two diagrams for the map (6) with $B = 0.5$ on the (A, C)-parameter plane. The panel (a) is the enlarged fragment of the right-bottom part of the Lyapunov diagram presented in Fig. 10c, and the panel (b) is the corresponding piece of a distance diagram depicting the distance between the attractor and the fixed point O_+. For the Lyapunov diagram we use the same color coding as in Sec. 3. Black color in the distance diagram corresponds to a small distance between the attractor and O_+ (the minimal distance less than 0.001 after 10^6 iterations of a point taken on the attractor), see the legend to the right of the panel (b). The top-right corner of Figs. 20 corresponds to the stability region of the point O_+, homoclinic attractors containing the saddle-focus fixed point O_+ of type (1,2) appear in the bottom-center region, colored in black at the panel (b). As one can see in the Lyapunov diagram, strange attractors here can be of three possible types: strongly dissipative (yellow color, $\Lambda_1 > 0$, $\Lambda_2 < 0$), hyperchaotic (red color, $\Lambda_1 > 0$, $\Lambda_2 > 0$), and flow-like (gray color, $\Lambda_1 > 0$, $\Lambda_2 \approx 0$).

Let us further fix $A = 1.33$ and study the scenario of the appearance of strange

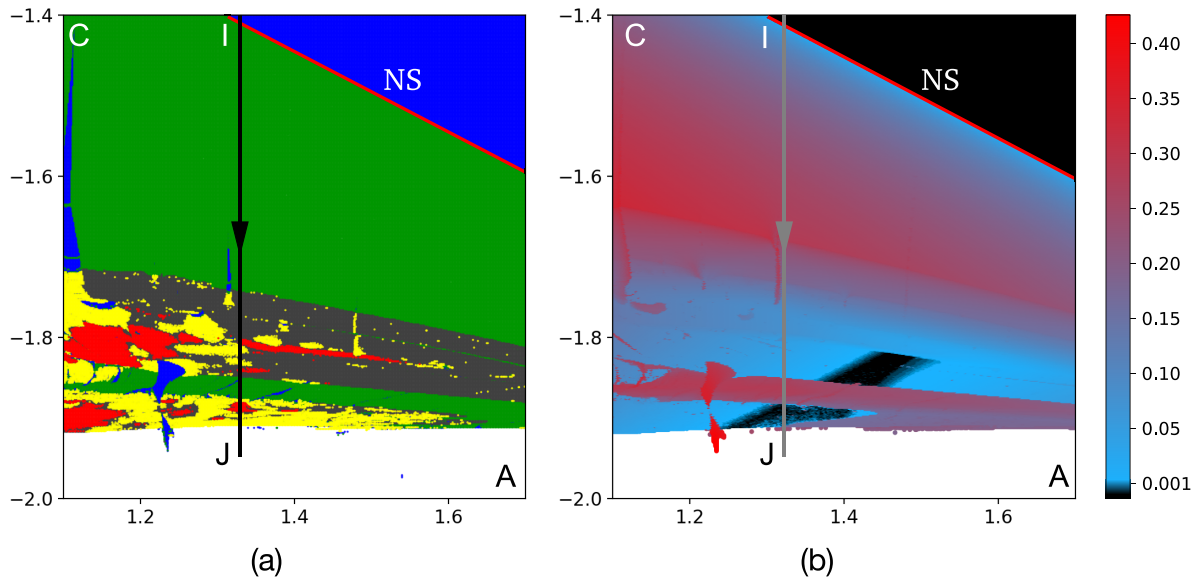

Figure 20: (A, C)-parameter diagrams for the map (6), $B = 0.5$. (a) Lyapunov diagram. (b) Diagram of the distance between the attractor and the fixed point O_+, in black colored regions this distance is less than 0.001. In the top-right region the point O_+ is asymptotically stable; homoclinic attractors containing the saddle-focus point O_+ of type (1,2) exist in the bottom-center region, colored in black in Fig. (b), they can be either hyperchaotic or not.

attractors along the pathway IJ: $(A = 1.33, B = 0.5)$. Results of the corresponding bifurcation analysis are shown in Figure 21. At the beginning, the stable fixed point O_+ is the only attractor of the map. Then, on the curve NS, this point undergoes the supercritical Neimark-Sacker bifurcation after which O_+ becomes saddle-focus of type (1,2) and the stable invariant curve L appears in its neighborhood, see Fig. 21a. Then, this curve undergoes two period-doubling (length-doubling) bifurcations. After the first period-doubling this curve becomes saddle and a stable doubled (2-round) invariant curve L^2 appears in its neighborhood. In its turn, the curve L^2 also undergoes the period-doubling bifurcation, it becomes saddle and a four-round stable invariant curve appears, see Fig. 21b. With further decrease in C, the four-round invariant curve breaks down, and, as a result, a torus-chaos attractor, possessing near-zero second Lyapunov exponent, is born, see Fig. 21c.

The graph of the distance between the attractor and the fixed point O_+, presented in Fig. 21f, shows that the attractor starts to contain O_+ at $C \approx -1.882$. Figure 22a, showing the transverse homoclinic structure for O_+, additionally confirms the inclusion of O_+ to the attractor. As it can be seen from the graph of Lyapunov exponents (Fig. 21e), the attractor becomes hyperchaotic on the interval $C \in (-1.89, -1.88)$. However, since the second Lyapunov exponent is slightly positive $(0 < \Lambda_2 < 0.006)$, hyperchaos here is very weak.

Moreover, the second Lyapunov exponent vanishes for chaotic attractors existing at some sufficiently large regions of the parameter space adjacent to the regions with homoclinic attractors. In order to see it, just superimpose the black-colored region in the bottom-center part of Fig. 20b with the corresponding part of the Lyapunov diagram.

Let us consider one more case for the appearance of the flow-like Shilnikov attractor in the map (6). Now we take $B = 0.7$, see the Lyapunov diagram in Fig. 10d and

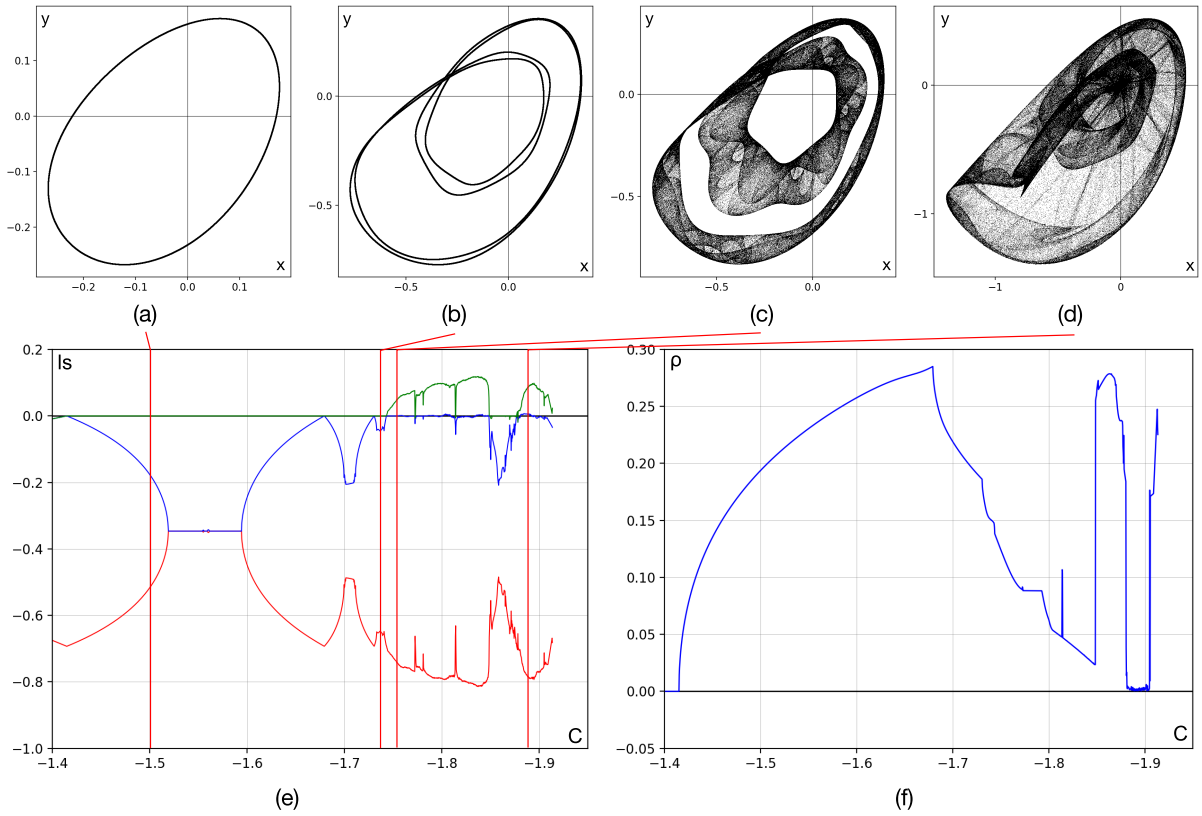

Figure 21: Evolution of attractors along the pathway IJ: ($B = 0.5, A = 1.33$). (a)–(d) phase portraits of the attractors: (a) $C = -1.5$ – stable invariant curve L; (b) $C = -1.732$ – four-round invariant curve; (c) $C = -1.75$ – torus-chaos attractor (LE: $\Lambda_1 = 0.033$, $\Lambda_2 = -3.65 \cdot 10^{-5}$, and $\Lambda_3 = -0.726$); (d) $C = -1.89$ – "weakly" hyperchaotic Shilnikov attractor (LE: $\Lambda_1 = 0.09$, $\Lambda_2 = 0.005$, and $\Lambda_3 = -0.788$). (e) the graph of Lyapunov exponents Λ_1, Λ_2, and Λ_3 on parameter C. (f) the graph of the distance between the attractor and the fixed point O_+.

its enlarged fragment near the right-bottom corner in Figure 23a. The corresponding distance diagram is presented in Figure 23b. Analyzing these figures, one can see that there are two regions where homoclinic attractors exist. However, non of these regions admit hyperchaotic attractors. Moreover, hyperchaotic attractors are not observable in this case at all, we find only flow-like chaotic attractors.

Let us consider the pathway KL: ($B = 0.7, A = 1.55$) and study bifurcations leading to the birth of homoclinic attractors in the left-bottom part of the diagrams presented in Fig. 23. Some results of the corresponding one-parameter bifurcation analysis are shown in Figure 24. In this case, the scenario for the appearance of the discrete Shilnikov attractor is almost the same as it was in the previous case, cf. Figs. 24a–24f with Figs. 21a–21f. The main difference between these two cases is that the stable invariant curve L undergoes here a quite long sequence of the period-doubling bifurcations before the destruction of the resulting multiround invariant curve.

Fig. 24g shows the corresponding bifurcation tree which we compute using the following scheme. We construct a Poincaré-like maps on the plane (x, z) introducing a cross-section box $|y| < 0.001$ in the phase space of the map. If a point of the attractor falls into this box we take its x-coordinate and plot on the graph $x(C)$. For each value of the parameter C we iterate the map 10000 times and plot the last 3000 points. The enlarged fragment of this bifurcation tree is shown in Fig. 24h. It is interesting to note that

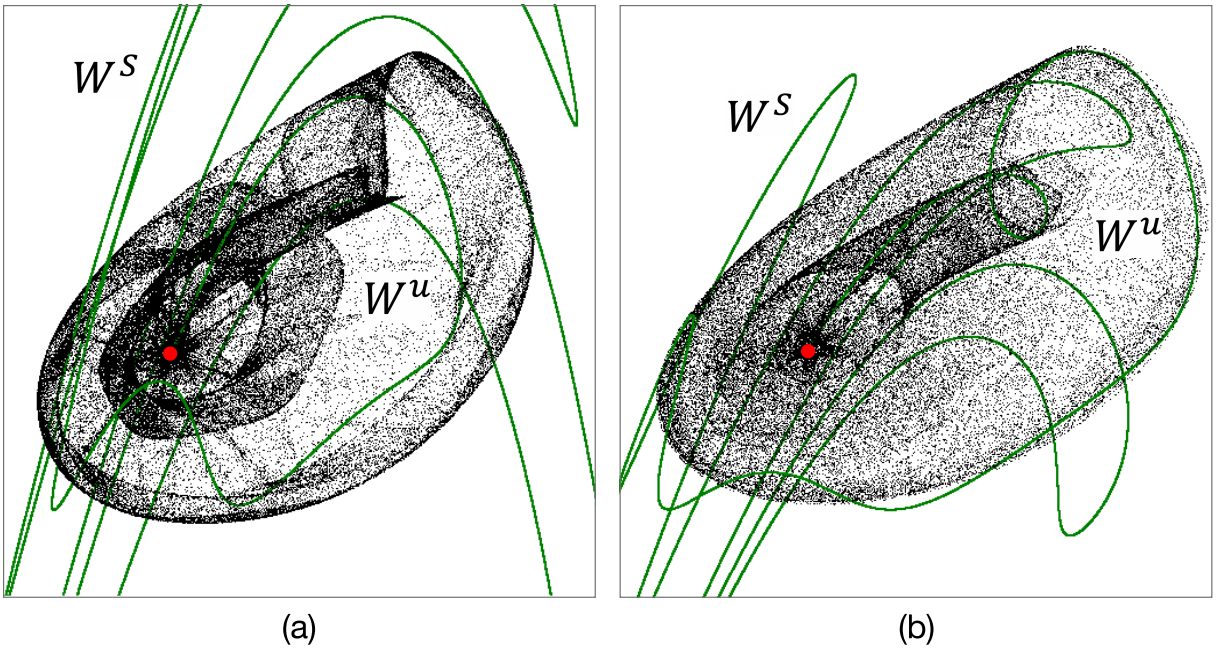

Figure 22: Phase portraits for different discrete Shilnikov attractors containing O_+: (a) $B = 0.5, A = 1.33, C = -1.89$ (LE: $\Lambda_1 = 0.09$, $\Lambda_2 = 0.005$, and $\Lambda_3 = -0.788$), (b) $B = 0.7, A = 1.55, C = -2.03$ (LE: $\Lambda_1 = 0.107$, $\Lambda_2 \approx 0$, and $\Lambda_3 = -0.463$). Green-colored curve is the branch of the stable invariant manifold of O_+ that forms the homoclinic intersection with the unstable manifold of O_+.

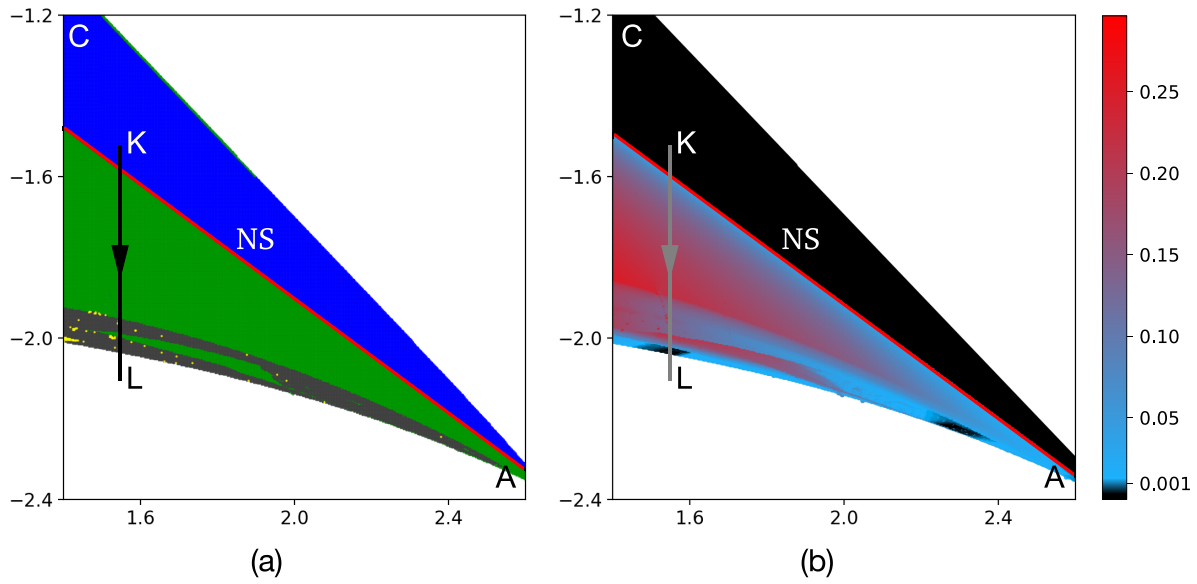

Figure 23: (A, C)-parameter diagrams for the map (6), $B = 0.7$. (a) Lyapunov diagram, the color scheme is the same as in Fig. 20a. (b) Diagram of the distance between the attractor and the fixed point O_+, in black colored regions this distance is less than 0.001. Homoclinic attractors containing the saddle-focus point O_+ of type (1,2) exist in the bottom regions, colored in black in panel (b). Almost all chaotic attractors observed here have one positive and one near-zero Lyapunov exponents.

the observed bifurcation tree looks like the well-known Feigenbaum tree [20] accompanying the formation of Hénon-like attractors. As it is known, such attractors often appear after the cascade of period-doubling bifurcations followed by the cascade of heteroclinic

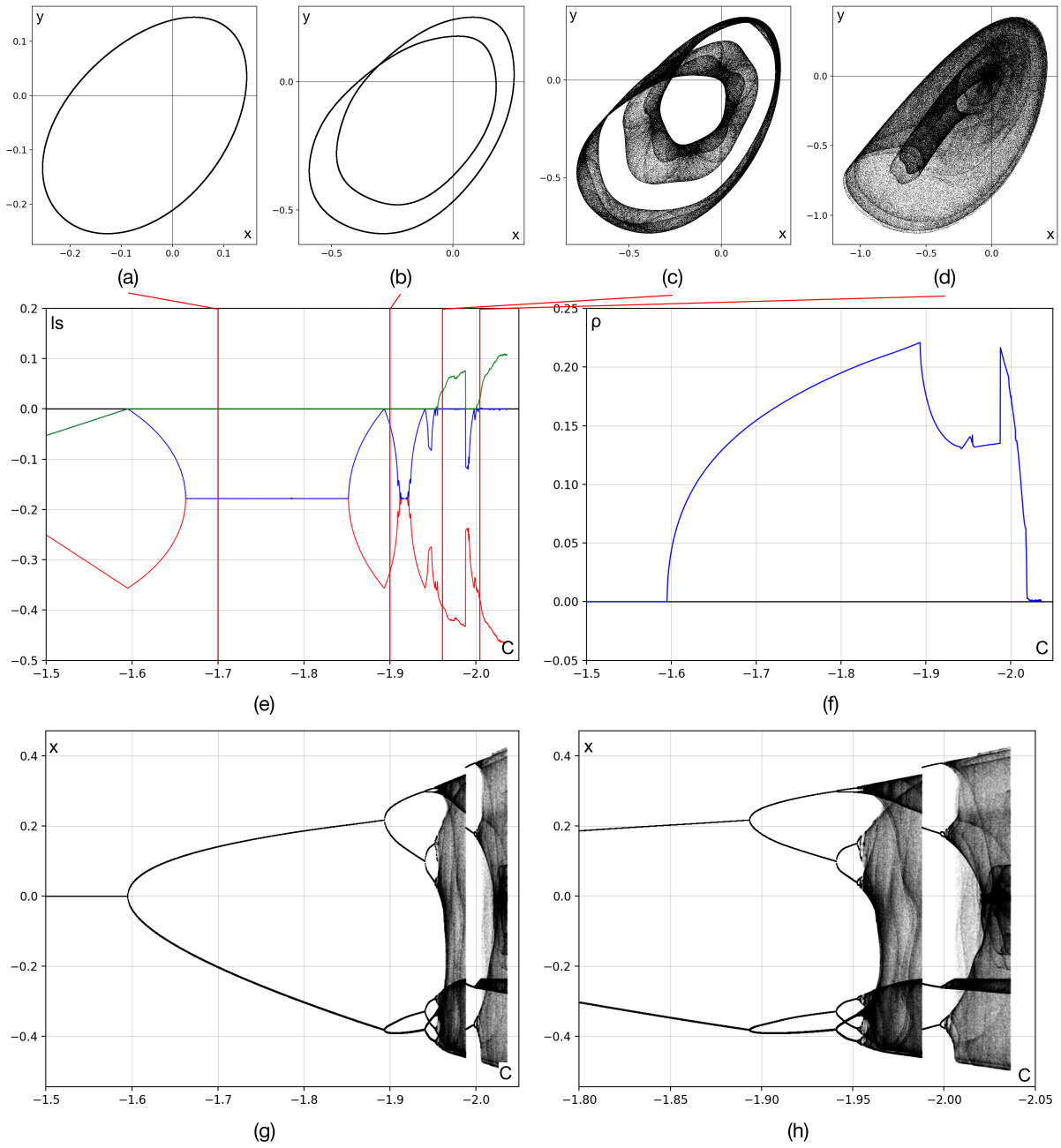

Figure 24: Evolution of the attractor along the pathway KL: ($B = 0.7, A = 1.55$). (a)–(d) phase portraits of the attractors: (a) $C = -1.7$ – stable invariant curve L;(b) $C = -1.9$ – doubled invariant curve; (c) $C = -1.96$ – torus-chaos attractor (LE: $\Lambda_1 = 0.0348$, $\Lambda_2 = 0.0001$, and $\Lambda_3 = -0.392$); (d) $C = -2.03$ – discrete Shilnikov attractor (LE: $\Lambda_1 = 0.107$, $\Lambda_2 \approx 0$, and $\Lambda_3 = -0.463$). (e) The graph of Lyapunov exponents Λ_1, Λ_2, and Λ_3 on parameter C. (f) the graph of the distance between the attractor and the fixed point O_+. (g) Bifurcation tree $x(C)$ computing with help of a Poincaré-like map on the plane (x, z) (using the cross-section box $|y| < 0.001$) and (f) its enlarged fragment.

band-fusion bifurcations which result in the absorption of periodic saddle orbits emerging after the corresponding period-doubling bifurcations. By the same manner, the sequence of the period-doubling bifurcations of a stable invariant curve leads to the appearance of a multicomponent chaotic attractor (on the corresponding two-dimensional Poincaré-like map) which, then, transforms to the one-component attractor via the sequence of hetero-

clinic bifurcations resulting in the absorption of the saddle invariant curves emerging after the corresponding period-doubling bifurcations. The resulting one-component attractor were called in [13–15] quasiperiodic Hénon-like attractor. It has one positive and one near-zero (indistinguishable from zero in numerics) Lyapunov exponents.

Finally, the chaotic attractor absorbs the saddle-focus fixed point O_+ of type (1,2), and the discrete Shilnikov flow-like attractor appears, see Fig. 24d. The corresponding homoclinic structure for O_+ is shown in Fig. 22b.

A natural questions arise here.

- Why does the second Lyapunov exponent is near-zero for chaotic attractors of the three-dimensional map inside large regions of the parameter space?
- Why do these attractors look like chaotic attractors of some three-dimensional system of differential equations, if the points on an orbit taken in the attractor are drawn not too densely?

The answer to these questions is quite simple. The flow-like chaotic attractors in the map (6) are observed close enough to the codimension-three bifurcation, when fixed point O_+ has the triplet of multipliers $(1, 1, 1)$: a pair of multipliers $\mu_{1,2}$ are equal to 1 at the resonance 1 : 1 bifurcation, where the curve NS intersects with the curve TR, while the third multiplier $\mu_3 = B$ is equal to one when the map is conservative (volume-preserving). It is not difficult to show that the asymptotic normal form for this codimension-three bifurcation in the case of the map (6) coincides with the well-known Arneodo-Coullet-Spiegel-Tresser (ACST) system

$$\begin{cases} \dot{x} = y, \\ \dot{y} = z, \\ \dot{z} = \alpha x + \beta y + \gamma z + x^2. \end{cases} \tag{10}$$

Bifurcation analysis for this system were performed in detail in Refs. [4, 5]. In particular, it was shown that Shilnikov attractors containing the saddle-focus equilibrium of type (1,2) with a homoclinic loop exist in this system. In Refs. [8, 30] it was described how such attractors are born from the stable equilibrium via chain of local and homoclinic bifurcations. At first, a stable equilibrium $Eq(0, 0, 0)$ undergoes the supercritical Andronov-Hopf bifurcation after which it becomes a saddle-focus and a stable limit cycle is born in its neighborhood, see Fig. 25a. Then, this cycle goes through the cascade of period-doubling bifurcations, see Fig. 25b. With further change in the control parameter, orbits of the attractor come closer and closer to the saddle-focus and, finally, Eq is included to the attractor, as a result of the appearance of Shilnikov homoclinic loop [72, 74], see Fig. 25c. As any chaotic attractor of a system of differential equations, this attractor has one positive and one zero Lyapunov exponents. This property is inherited by the map (6) in some (sufficiently large) neighborhood of the codimension-three bifurcation when the fixed point O_+ has the triplet of multipliers $(1, 1, 1)$.[8]

[8]Similar phenomenon of the existence of flow-like chaotic attractors was previously discovered and studied in Ref. [36] for the 3D Hénon map $\bar{x} = y,\ \bar{y} = z,\ \bar{z} = M_1 + Bx + M_2 y - z^2$ possessing the discrete Lorenz attractor (with near-zero second Lyapunov exponent) in an open large region of the (M_1, M_2, B)-parameter space adjacent to the codimension-three point when a fixed point of the map has multipliers $(-1, -1, 1)$. The 3D Hénon map appears as a normal form for the first-return map near a quadratic

If to compare phase portraits of the attractor found in the map (6) at $B = 0.7$ (Fig. 22b) and the attractor presented in Fig. 25c, it is easy to conclude that these attractors are similar. An orbit taken in the first attractor looks like a discretization of a continuous orbit taken in the second attractor.

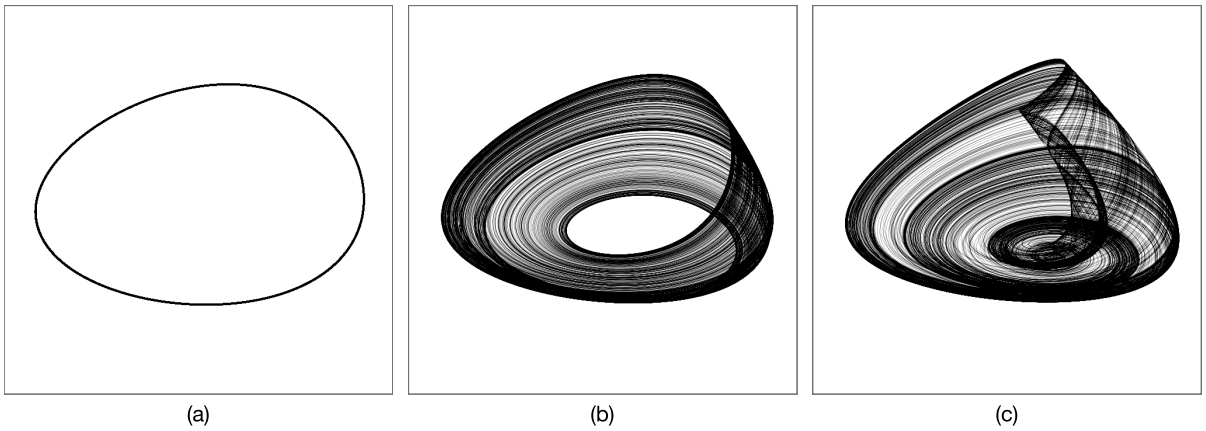

Figure 25: Main steps towards the Shilnikov attractor appearance in the system (10) for $C = -0.4, B = -1$: (a) $A = -0.7$, stable limit cycle, (b) $A = -0.8$, Rössler-like attractor, (c) $A = -0.87$, Shilnikov spiral attractor.

7 Discussion

We have proposed bifurcation scenarios leading from a stable fixed point to a hyperchaotic attractor in one-parameter families of three-dimensional maps and have applied them for studying the formation of hyperchaotic attractors in the three-dimensional Mirá map (1). These scenarios consist of two parts. The first part describes a few main bifurcations resulting in the appearance of a homoclinic attractor containing saddle fixed point of type (1,2). The second part describes accompanying bifurcations after which the majority of orbits inside the attractor get the two-dimensional unstable manifolds.

For the map (1) we have shown that the part is the extension of the well-known Shilnikov scenario [75] to the case of three-dimensional maps [26, 27, 31]. In the framework of this scenario, a stable fixed point O_+ undergoes the supercritical Neimark-Sacker and the stable invariant curve L appears in its neighborhood. Then, this curve breaks down giving a torus-chaos attractor with the isolated saddle-focus point O_+ of type (1,2). The final part of the scenario is the inclusion (absorption) of this point by the attractor. The resulting discrete Shilnikov attractor contains this point.

The second part of the scenario describes mechanisms of the destruction of the curve L. Usually, before the destruction, this curve becomes resonant. We have shown that depending on values of the parameters the corresponding resonant orbits can give rise to hyperchaotic periodic orbits of type (1,2) in two different ways:

(i) the stable resonant orbit undergoes the cascade of period-doubling bifurcations. (This cascade can be interrupted by the supercritical Neimark-Sacker bifurcation.

homoclinic tangency to a saddle-focus fixed point with the Jacobian closed to 1 [33]. Also note that this map is the inverse to the 3D Mirá map (1). Therefore, in the map (1) there exists a discrete Lorenz repeller (with near-zero second Lyapunov exponent) for $B > 1$.

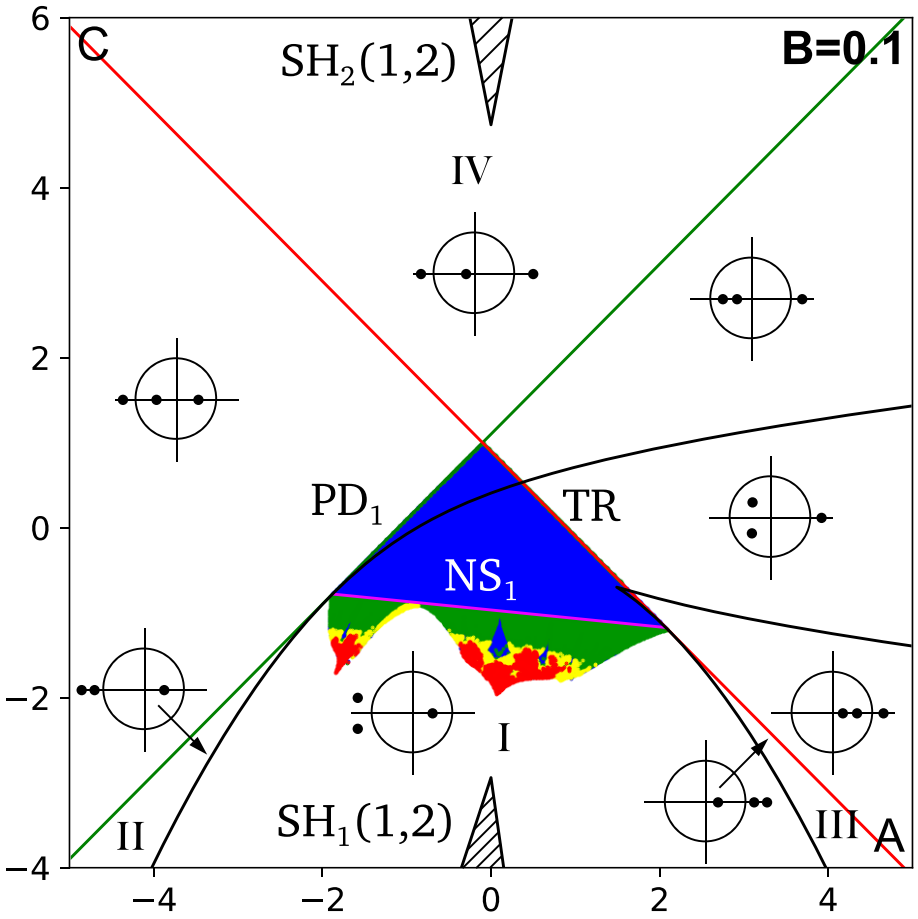

Figure 26: Saddle chart superimposed with the Lyapunov diagram for the map (6), $B = 0.1$. In the regions $SH_{1,2}(1,2)$ the nonwandering set of the map is nontrivial hyperbolic of type (1,2). Hyperchaotic homoclinic attractors of different types are possible in regions I–IV.

In this case, see option (ii)). In their turn, the resulting periodic saddle orbits of type (2,1), as well as the resonant saddle orbits of type (2,1) undergo the cascade of period-doubling bifurcations transforming the corresponding periodic orbits to saddles of type (1,2).

(ii) the stable resonant orbit undergoes the supercritical Neimark-Sacker bifurcation transforming this orbit to the saddle-focus of type (1,2) and a stable multicomponent invariant curve appears. At some moment, this invariant curve (as the curve L) becomes resonant, option (i) or (ii) is realized and so on. The saddle resonant orbits, as well as in case (i), undergo the cascades of period-doubling bifurcations.

In both cases, the attractor absorbs the sets of periodic saddle orbits of type (1,2) and becomes hyperchaotic.

In the paper, we have also proposed a new scenario leading to the creation of the so-called hyperchaotic Hénon-like attractor containing a saddle fixed point with a pair of negative unstable multipliers,

Finally, we would like to note one more interesting property of the map (6). One of its fixed points is always fixed at the origin and its eigenvalues depend only on the parameters

A, B, and C. In Figure 26, we show the extended bifurcation diagram for this fixed point (when $B = 0.1$) above the Lyapunov diagram. Such extended diagrams were called *saddle charts* in [27]. In this diagram one can see four regions with possible hyperchaotic homoclinic attractors: the region I – with the discrete Shilnikov attractor, the region II – with the hyperchaotic Hénon-like attractor, the region III – with a hyperchaotic attractor containing a fixed point with a pair of positive unstable multipliers and the region IV – with a hyperchaotic attractor containing a fixed point with a pair of real unstable multipliers with different signs. Varying nonlinear terms in the map we can expect new types of hyperchaotic homoclinic attractors. This problem looks very promising, especially for the region IV, inside which, as well as inside the region I, by Gonchenko and Li theorem [29], the nonwandering set of the map is the Smale horseshoe of type (1,2). Thus, one can expect the existence of hyperchaotic attractors in IV for quite general families of the three-dimensional Hénon maps.

Acknowledgements

The authors thank Sergey Gonchenko, Igor Sataev, and Dmitry Turaev for fruitful discussions. The authors also express their gratitude to the Referee and Editors for valuable comments, which significantly helped to improve this paper.

This work was carried out with the support of the RSF grant No. 19-71-10048 (Sections 4 and 5) and the Basic Research Program at HSE University (Sections 2, 3, and 6). A. Kazakov and E. Karatetskaia also acknowledge Theoretical Physics and Mathematics Advancement Foundation BASIS for the support of scientific research.

References

[1] V. Afraimovich and L. Shilnikov. "Invariant two-dimensional tori, their breakdown and stochasticity". In: *Amer. Math. Soc. Transl* 149.2 (1991), pp. 201–212.

[2] V. Anishchenko and S. Nikolaev. "Generator of quasi-periodic oscillations featuring two-dimensional torus doubling bifurcations". In: *Technical physics letters* 31.10 (2005), pp. 853–855.

[3] A. Arneodo, P. Coullet, and E. Spiegel. "Cascade of period doublings of tori". In: *Physics Letters A* 94.1 (1983), pp. 1–6.

[4] A. Arneodo, P. Coullet, and E. Spiegel. "The dynamics of triple convection". In: *Geophysical & Astrophysical Fluid Dynamics* 31.1–2 (1985), pp. 1–48.

[5] A. Arneodo, P. Coullet, E. Spiegel, and C. Tresser. "Asymptotic chaos". In: *Physica D: Nonlinear Phenomena* 14.3 (1985), pp. 327–347.

[6] S. Aubry. "Anti-integrability in dynamical and variational problems". In: *Physica D: Nonlinear Phenomena* 86.1–2 (1995), pp. 284–296.

[7] G. Baier and M. Klein. "Maximum hyperchaos in generalized Hénon maps". In: *Physics Letters A* 151.6-7 (1990), pp. 281–284.

[8] Y. V. Bakhanova, S. Gonchenko, A. Gonchenko, A. Kazakov, and E. Samylina. "On Shilnikov attractors of three-dimensional flows and maps". In: *Journal of Difference Equations and Applications* (2022), pp. 1–18.

[9] A. Barugola, J.-c. Cathala, L. Gardini, and C. Mira. *Chaotic dynamics in two-dimensional noninvertible maps*. Vol. 20. World Scientific, 1996.

[10] M. Benedicks and L. Carleson. "The dynamics of the Hénon map". In: *Annals of Mathematics* 133.1 (1991), pp. 73–169.

[11] G. Benettin, L. Galgani, A. Giorgilli, and J.-M. Strelcyn. "Lyapunov characteristic exponents for smooth dynamical systems and for Hamiltonian systems; a method for computing all of them. Part 1: Theory". In: *Meccanica* 15.1 (1980), pp. 9–20.

[12] A. V. Borisov, A. O. Kazakov, and I. R. Sataev. "Spiral chaos in the nonholonomic model of a Chaplygin top". In: *Regular and Chaotic Dynamics* 21.7–8 (2016), pp. 939–954.

[13] H. Broer, C. Simó, and R. Vitolo. "Bifurcations and strange attractors in the Lorenz-84 climate model with seasonal forcing". In: *Nonlinearity* 15.4 (2002), p. 1205.

[14] H. W. Broer, C. Simó, and R. Vitolo. "Chaos and quasi-periodicity in diffeomorphisms of the solid torus". In: *Discrete Contin. Dyn. Syst. Ser. B* 14.3 (2010), pp. 871–905.

[15] H. Broer, R. Vitolo, and C. Simó. "Quasi-periodic Hénon-like attractors in the Lorenz-84 climate model with seasonal forcing". In: *EQUADIFF 2003*. World Scientific, 2005, pp. 601–606.

[16] M. Campanino and H. Epstein. "On the existence of Feigenbaum's fixed point". In: *Communications in Mathematical Physics* 79.2 (1981), pp. 261–302.

[17] P. Collet, J. Eckmann, and H. Koch. "Period Doubling Bifurcations for Families of Maps on R^n". In: *Journal of Statistical Physics* 25 (1981), pp. 1–14.

[18] A. De Carvalho, M. Lyubich, and M. Martens. "Renormalization in the Hénon family, I: Universality but non-rigidity". In: *Journal of Statistical Physics* 121.5-6 (2005), pp. 611–669.

[19] J.-P. Eckmann and P. Wittwer. "A complete proof of the Feigenbaum conjectures". In: *Journal of statistical physics* 46.3 (1987), pp. 455–475.

[20] M. J. Feigenbaum. "Quantitative universality for a class of nonlinear transformations". In: *Journal of statistical physics* 19.1 (1978), pp. 25–52.

[21] Z. Galias and W. Tucker. "Is the Hénon attractor chaotic?" In: *Chaos: An Interdisciplinary Journal of Nonlinear Science* 25.3 (2015), p. 033102.

[22] J.-M. Gambaudo, S. van Strien, and C. Tresser. "Hénon-like maps with strange attractors: there exist C_∞ Kupka-Smale diffeomorphisms on S^2 with neither sinks nor sources". In: *Nonlinearity* 2.2 (1989), p. 287.

[23] I. R. Garashchuk, D. I. Sinelshchikov, A. O. Kazakov, and N. A. Kudryashov. "Hyperchaos and multistability in the model of two interacting microbubble contrast agents". In: *Chaos: An Interdisciplinary Journal of Nonlinear Science* 29.6 (2019), p. 063131.

[24] R. K. Ghaziani, W. Govaerts, and C. Sonck. "Resonance and bifurcation in a discrete-time predator-prey system with Holling functional response". In: *Nonlinear Analysis: Real World Applications* 13.3 (2012), pp. 1451–1465.

[25] J. Gheiner. "Codimension-two reflection and non-hyperbolic invariant lines". In: *Nonlinearity* 7.1 (1994), p. 109.

[26] A. Gonchenko, S. Gonchenko, A. Kazakov, and D. Turaev. "Simple scenarios of onset of chaos in three-dimensional maps". In: *International Journal of Bifurcation and Chaos* 24.08 (2014), p. 1440005.

[27] A. Gonchenko and S. Gonchenko. "Variety of strange pseudohyperbolic attractors in three-dimensional generalized Hénon maps". In: *Physica D: Nonlinear Phenomena* 337 (2016), pp. 43–57.

[28] A. Gonchenko, S. Gonchenko, A. Kazakov, and E. Samylina. "Chaotic dynamics and multistability in the nonholonomic model of a Celtic stone". In: *Radiophysics and Quantum Electronics* 61.10 (2019), pp. 773–786.

[29] S. Gonchenko and M.-C. Li. "Shilnikov's cross-map method and hyperbolic dynamics of three-dimensional Hénon-like maps". In: *Regular and Chaotic Dynamics* 15.2-3 (2010), pp. 165–184.

[30] S. V. Gonchenko, A. S. Gonchenko, A. O. Kazakov, A. D. Kozlov, and Y. V. Bakhanova. "Mathematical theory of dynamical chaos and its applications: Review. Part 2. Spiral chaos of three-dimensional flows". In: *Izvestiya VUZ. Applied Nonlinear Dynamics* 27.5 (2019), pp. 7–52.

[31] S. V. Gonchenko, A. S. Gonchenko, and L. P. Shilnikov. "Towards scenarios of chaos appearance in three-dimensional maps". In: *Rus. J. Nonlin. Dyn* 8.1 (2012), pp. 3–28.

[32] S. V. Gonchenko, V. S. Gonchenko, and L. P. Shilnikov. "On a homoclinic origin of Hénon-like maps". In: *Regular and Chaotic Dynamics* 15.4-5 (2010), pp. 462–481.

[33] S. V. Gonchenko, J. D. Meiss, and I. I. Ovsyannikov. "Chaotic dynamics of three-dimensional Hénon maps that originate from a homoclinic bifurcation". In: *Regular and Chaotic Dynamics* 11.2 (2006), pp. 191–212.

[34] S. V. Gonchenko, D. V. Turaev, and L. P. Shilnikov. "Dynamical phenomena in multidimensional systems with a structurally unstable homoclinic Poincaré curve". In: *Doklady Akademii Nauk* 330.2 (1993), pp. 144–147.

[35] S. V. Gonchenko, D. V. Turaev, and L. P. Shilnikov. "On the existence of Newhouse regions in a neighborhood of systems with a structurally unstable homoclinic Poincaré curve (the multidimensional case)". In: *Doklady Akademii Nauk* 329.4 (1993), pp. 404–407.

[36] S. V. Gonchenko, I. I. Ovsyannikov, C. Simó, and D. Turaev. "Three-dimensional Hénon-like maps and wild Lorenz-like attractors". In: *International Journal of Bifurcation and Chaos* 15.11 (2005), pp. 3493–3508.

[37] S. V. Gonchenko, L. P. Shilnikov, and D. V. Turaev. "On dynamical properties of multidimensional diffeomorphisms from Newhouse regions: I". In: *Nonlinearity* 21.5 (2008), p. 923.

[38] S. Gonchenko, L. Shilnikov, and D. Turaev. "Dynamical phenomena in systems with structurally unstable Poincaré homoclinic orbits". In: *Chaos: An Interdisciplinary Journal of Nonlinear Science* 6.1 (1996), pp. 15–31.

[39] S. Gonchenko, L. Shilnikov, and D. Turaev. "Quasiattractors and homoclinic tangencies". In: *Computers & Mathematics with Applications* 34.2-4 (1997), pp. 195–227.

[40] W. Govaerts, Y. A. Kuznetsov, and H. Meijer. *MatContM: Numerical Bifurcation Analysis Toolbox in Matlab*. 2020.

[41] W. Govaerts and R. K. Ghaziani. "Stable cycles in a Cournot duopoly model of Kopel". In: *Journal of Computational and Applied Mathematics* 218.2 (2008), pp. 247–258.

[42] E. A. Grines, A. Kazakov, and I. R. Sataev. "On the origin of chaotic attractors with two zero Lyapunov exponents in a system of five biharmonically coupled phase oscillators". In: *Chaos: An Interdisciplinary Journal of Nonlinear Science* 32.9 (2022), p. 093105.

[43] A. E. Hampton and J. D. Meiss. "Anti-integrability for Three-Dimensional Quadratic Maps". In: *SIAM Journal on Applied Dynamical Systems* 21.1 (2022), pp. 650–675.

[44] A. E. Hampton and J. D. Meiss. "The three-dimensional generalized Hénon map: Bifurcations and attractors". In: *Chaos: An Interdisciplinary Journal of Nonlinear Science* 32.11 (2022), p. 113127.

[45] M. Hénon. "A two-dimensional mapping with a strange attractor". In: *The Theory of Chaotic Attractors*. Springer, 1976, pp. 94–102.

[46] J. Juang, M.-C. Li, and M. Malkin. "Chaotic difference equations in two variables and their multidimensional perturbations". In: *Nonlinearity* 21.5 (2008), p. 1019.

[47] K. Kaneko. "Doubling of torus". In: *Progress of theoretical physics* 69.6 (1983), pp. 1806–1810.

[48] T. Kapitaniak, Y. Maistrenko, and S. Popovych. "Chaos-hyperchaos transition". In: *Physical Review E* 62.2 (2000), p. 1972.

[49] M. Komuro, K. Kamiyama, T. Endo, and K. Aihara. "Quasi-periodic bifurcations of higher-dimensional tori". In: *International Journal of Bifurcation and Chaos* 26.07 (2016), p. 1630016.

[50] M. Kopel. "Simple and complex adjustment dynamics in Cournot duopoly models". In: *Chaos, Solitons & Fractals* 7.12 (1996), pp. 2031–2048.

[51] A. G. Korotkov, A. O. Kazakov, and T. A. Levanova. "Effects of memristor-based coupling in the ensemble of FitzHugh–Nagumo elements". In: *The European Physical Journal Special Topics* 228.10 (2019), pp. 2325–2337.

[52] A. Kuznetsov, S. Kuznetsov, and I. Sataev. "A variety of period-doubling universality classes in multi-parameter analysis of transition to chaos". In: *Physica D: Nonlinear Phenomena* 109.1-2 (1997), pp. 91–112.

[53] Y. A. Kuznetsov, H. G. Meijer, and L. van Veen. "The fold-flip bifurcation". In: *International Journal of Bifurcation and Chaos* 14.07 (2004), pp. 2253–2282.

[54] Y. A. Kuznetsov. "A Tutorial for MatcontM GUI". In: *Utretcht University, Utrecht* (2013).

[55] Y. A. Kuznetsov and H. G. Meijer. *Numerical Bifurcation Analysis of Maps*. Vol. 34. Cambridge University Press, 2019.

[56] O. E. Lanford. "A computer-assisted proof of the Feigenbaum conjectures". In: *Bull. Amer. Math. Soc* 6.3 (1982), pp. 427–434.

[57] D. Li. "Homoclinic bifurcations that give rise to heterodimensional cycles near a saddle-focus equilibrium". In: *Nonlinearity* 30.1 (2016), p. 173.

[58] D. Li and D. Turaev. "Existence of heterodimensional cycles near Shilnikov loops in systems with a Z_2 symmetry". In: *Discrete and Continuous Dynamical Systems Seria A* 37.8 (2017), pp. 4399–4437.

[59] D. Li and D. Turaev. "Persistent heterodimensional cycles in periodic perturbations of Lorenz-like attractors". In: *Nonlinearity* 33.3 (2020), p. 971.

[60] M.-C. Li and M. Malkin. "Topological horseshoes for perturbations of singular difference equations". In: *Nonlinearity* 19.4 (2006), p. 795.

[61] H. E. Lomelí and J. D. Meiss. "Quadratic volume-preserving maps". In: *Nonlinearity* 11.3 (1998), p. 557.

[62] M. Lyubich and M. Martens. "Renormalization in the Hénon family, II: The heteroclinic web". In: *Inventiones mathematicae* 186.1 (2011), pp. 115–189.

[63] F. Marotto. "Snap-back repellers imply chaos in R^N". In: *Journal of Mathematical Analysis and Applications* 63 (1978), pp. 199–223.

[64] H. Meijer, W. Govaerts, Y. A. Kuznetsov, R. K. Ghaziani, and N. Neirynck. *MatContM, A toolbox for continuation and bifurcation of cycles of maps: Command line use*. 2017.

[65] C. Mira. "Determination pratique du domaine de stabilite dún point déquilibre dúne recurrence nonlineaire". In: 261 (1965), pp. 5314–5317.

[66] J. D. Mireles James. "Quadratic volume-preserving maps: (un)stable manifolds, hyperbolic dynamics, and vortex-bubble bifurcations". In: *Journal of Nonlinear Science* 23.4 (2013), pp. 585–615.

[67] M. Misiurewicz and P. Zgliczyński. "Topological entropy for multidimensional perturbations of one-dimensional maps". In: *International Journal of Bifurcation and Chaos* 11.05 (2001), pp. 1443–1446.

[68] W.-X. Qin. "Chaotic invariant sets of high-dimensional Hénon-like maps". In: *Journal of mathematical analysis and applications* 264.1 (2001), pp. 76–84.

[69] H. Richter. "The generalized Henon maps: Examples for higher-dimensional chaos". In: *International Journal of Bifurcation and Chaos* 12.06 (2002), pp. 1371–1384.

[70] O. E. Rössler. "An equation for hyperchaos". In: *Physics Letters A* 71.2-3 (1979), pp. 155–157.

[71] I. Sataev and N. Stankevich. "Cascade of torus birth bifurcations and inverse cascade of Shilnikov attractors merging at the threshold of hyperchaos". In: *Chaos: An Interdisciplinary Journal of Nonlinear Science* 31.2 (2021), p. 023140.

[72] L. P. Shilnikov. "A case of the existence of a denumerable set of periodic motions". In: *Doklady Akademii Nauk* 160.3 (1965), pp. 558–561.

[73] L. P. Shilnikov. "On a Poincaré–Birkhoff problem". In: *Matematicheskii Sbornik* 116.3 (1967), pp. 378–397.

[74] L. P. Shilnikov and A. Shilnikov. "Shilnikov bifurcation". In: *Scholarpedia* 2.8 (2007), p. 1891.

[75] L. Shilnikov. "The theory of bifurcations and turbulence". In: *Selecta Math. Sovietica* 10 (1991), pp. 43–53.

[76] C. Simó and A. Vieiro. "Resonant zones, inner and outer splittings in generic and low order resonances of area preserving maps". In: *Nonlinearity* 22.5 (2009), p. 1191.

[77] C. Simó. "On the Hénon-Pomeau attractor". In: *Journal of Statistical Physics* 21.4 (1979), pp. 465–494.

[78] S. Smale. "Differentiable dynamical systems". In: *Bulletin of the American mathematical Society* 73.6 (1967), pp. 747–817.

[79] N. Stankevich, A. Kazakov, and S. Gonchenko. "Scenarios of hyperchaos occurrence in 4D Rössler system". In: *Chaos: An Interdisciplinary Journal of Nonlinear Science* 30.12 (2020), p. 123129.

[80] N. Stankevich, N. Shchegoleva, I. Sataev, and A. Kuznetsov. "Three-dimensional torus breakdown and chaos with two zero Lyapunov exponents in coupled radiophysical generators". In: *Journal of Computational and Nonlinear Dynamics* 15.11 (2020).

[81] N. Stankevich and E. Volkov. "Chaos–hyperchaos transition in three identical quorum-sensing mean-field coupled ring oscillators". In: *Chaos: An Interdisciplinary Journal of Nonlinear Science* 31.10 (2021), p. 103112.

[82] D. V. Turaev and L. P. Shilnikov. "An example of a wild strange attractor". In: *Sbornik: Mathematics* 189.2 (1998), p. 291.

[83] D. Turaev and L. Shilnikov. "Pseudohyperbolicity and the problem on periodic perturbations of Lorenz-type attractors". In: *Doklady Mathematics* 77.1 (2008), p. 17.

[84] S. Yanchuk and T. Kapitaniak. "Chaos–hyperchaos transition in coupled Rössler systems". In: *Physics Letters A* 290.3-4 (2001), pp. 139–144.

[85] S. Yanchuk and T. Kapitaniak. "Symmetry-increasing bifurcation as a predictor of a chaos-hyperchaos transition in coupled systems". In: *Physical Review E* 64.5 (2001), p. 056235.

[86] X. Zhang. "Chaotic polynomial maps". In: *International Journal of Bifurcation and Chaos* 26.08 (2016), p. 1650131.

[87] M. Zhao, C. Li, J. Wang, and Z. Feng. "Bifurcation analysis of the three-dimensional Hénon map". In: *Discrete & Continuous Dynamical Systems-S* 10.3 (2017), p. 625.

[88] Z. T. Zhusubaliyev, J. L. Laugesen, and E. Mosekilde. "From multi-layered resonance tori to period-doubled ergodic tori". In: *Physics Letters A* 374.25 (2010), pp. 2534–2538.

[89] Z. T. Zhusubaliyev and E. Mosekilde. "Formation and destruction of multilayered tori in coupled map systems". In: *Chaos: An Interdisciplinary Journal of Nonlinear Science* 18.3 (2008), p. 037124.

[90] Z. T. Zhusubaliyev and E. Mosekilde. "Novel routes to chaos through torus breakdown in non-invertible maps". In: *Physica D: Nonlinear Phenomena* 238.5 (2009), pp. 589–602.